Hydrogeol J (2017) 25:421–444
DOI 10.1007/s10040-016-1496-6

PAPER

Preferential flow, diffuse flow, and perching in an interbedded fractured-rock unsaturated zone

John R. Nimmo[1] **· Kaitlyn M. Creasey**[1] **· Kim S. Perkins**[1] **· Benjamin B. Mirus**[2]

Received: 20 April 2016 / Accepted: 8 November 2016 / Published online: 26 November 2016

Abstract Layers of strong geologic contrast within the unsaturated zone can control recharge and contaminant transport to underlying aquifers. Slow diffuse flow in certain geologic layers, and rapid preferential flow in others, complicates the prediction of vertical and lateral fluxes. A simple model is presented, designed to use limited geological site information to predict these critical subsurface processes in response to a sustained infiltration source. The model is developed and tested using site-specific information from the Idaho National Laboratory in the Eastern Snake River Plain (ESRP), USA, where there are natural and anthropogenic sources of high-volume infiltration from floods, spills, leaks, wastewater disposal, retention ponds, and hydrologic field experiments. The thick unsaturated zone overlying the ESRP aquifer is a good example of a sharply stratified unsaturated zone. Sedimentary interbeds are interspersed between massive and fractured basalt units. The combination of surficial sediments, basalts, and interbeds determines the water fluxes through the variably saturated subsurface. Interbeds are generally less conductive, sometimes causing perched water to collect above them. The model successfully predicts the volume and extent of perching and approximates vertical travel times during events that generate high fluxes from the land surface. These developments are applicable to sites having a thick, geologically complex unsaturated zone of substantial thickness in which preferential and diffuse flow, and perching of percolated water, are important to contaminant transport or aquifer recharge.

Keywords Unsaturated zone · Preferential flow · Perched water · Fractured basalt · Impeding layers

Introduction

In many regions of the world, the unsaturated zone is tens of meters or more thick and geologically complex, comprising diverse strata that typically are heterogeneous within themselves at multiple scales. Effective water management in these regions requires increased knowledge of hydraulic processes in the unsaturated zone, which quantitatively link precipitation, infiltration, and percolation to the underlying aquifer.

Geologic stratification in the unsaturated zone has diverse hydrologic effects. It can retard downward unsaturated flow because of individual layers that conduct poorly or, regardless of which layer is more conductive, because of the retarding effect of layer contrasts (Miller and Gardner 1962; Nimmo and Perkins 2008). Conversely, it can cause flow instabilities that generate fingers of relatively rapid flow (Hill and Parlange 1972; Hendrickx and Flury 2001). Flow impedances associated with layer contrasts or low-conductivity layers sometimes cause perched water to collect above them. These thin but laterally extensive saturated volumes can lead to greatly enhanced, or possibly impeded, transport of water and contaminants (e.g. Hammermeister et al. 1982; Oostrom et al. 2013). They complicate subsurface transport with saturated/unsaturated interactions and increased likelihood and magnitude of lateral flows.

This paper quantitatively evaluates the phenomena of perching and preferential flow, both of which exert major control over recharging fluxes, contaminant transport, and

✉ John R. Nimmo
jrnimmo@usgs.gov

[1] US Geological Survey, 345 Middlefield Road, MS 420, Menlo Park, CA 94025, USA

[2] US Geological Survey, 1711 Illinois Street, MS 966, Golden, CO 80401, USA

hydrologic water balance. When both occur, each amplifies the importance of the other.

The Eastern Snake River Plain (ESRP) in Idaho, USA, having a large and heavily utilized aquifer, multiple alternating basaltic and sedimentary layers, and an unsaturated zone of thickness up to 200 m or more, provides an important study site for these processes and issues (Barraclough et al. 1967; Nimmo et al. 2004; Smith 2004). Layers in both the unsaturated zone and aquifer mostly are either fine, unconsolidated sediments or fractured rock. (Here the term "fractured rock" is used to include associated rock composed of unconsolidated fragments, for example rubble or gravel zones.) A major advantage of this location is that previous investigations have produced an extensive data record of water flow dynamics in the unsaturated zone and aquifer (Barraclough et al. 1967; Rightmire and Lewis 1987; Anderson and Liszewski 1997; Dunnivant et al. 1998; Perkins and Nimmo 2000; Nimmo et al. 2002; Duke et al. 2007; Mirus et al. 2011). Geologic and hydraulic property data from recent USGS investigations (Perkins et al. 2014; Twining et al. 2014) at an ESRP location referred to as USGS 140/141 (Fig. 1) within the Idaho National Laboratory (INL) provide an opportunity to explore new methods for characterizing preferential flow and perching phenomena in combination with the more frequently studied diffuse flows, and to use them to learn about this previously little-explored portion of the unsaturated zone.

Diffuse and preferential flow

Unsaturated zone flow is often treated as having either diffuse or preferential character. Through sediments, at the ESRP and other sites with deep unsaturated zones, unsaturated flow is commonly diffuse, though preferential flow also can occur. Through fractured rock with little matrix porosity, essentially all flow is preferential.

Diffuse flow, considered as progressing through connected pores, each of which departs only slightly, and in diminishing degree, from equilibrium with those in its vicinity, can generally be quantified using traditional theory embodied in such relationships as the Darcy-Buckingham Law and Richards' equation. It normally entails slow transport processes with the possibility of strong interactions between water and solid materials.

Preferential flow moves rapidly through narrow pathways in disequilibrium with the surrounding matrix material, in contrast to slower diffuse flow, which moves through broad regions of matrix material. It can speed transport of contaminants through the unsaturated zone while exposing them to only a small fraction of the natural subsurface materials, thereby reducing the opportunity for chemical reactions and adsorption. Preferential flow commonly occurs due to elongated pores or fractures, fingering caused by flow instability, or heterogeneities at small or intermediate scales. It becomes more prevalent in situations of stratification, perching, heterogeneity, and geologic complexity. Though of great practical concern, preferential flow is poorly understood at both fundamental and practical levels (Pruess 1998; Jarvis 2007). This poor understanding is apparent in the lack of a widely accepted quantitative model for preferential flow, whether occurring as the dominant mode on its own, or in combination with diffuse flow. Of several different types of quantitative models in use, none is universally accepted (Beven and Germann 2013). Most approaches consider two domains of the unsaturated medium. Normally one domain has diffuse flow quantifiable with Darcy-Buckingham and Richards formulations, with traditional hydraulic conductivity and water retention properties to represent the medium. Various alternatives are used for the preferential domain, including Richards' equation applied with property values different from those used for the diffuse domain (Gerke and van Genuchten 1993), kinematic waves (Larsbo and Jarvis 2003) and others, including the source-responsive flow (Nimmo 2010) used in this study.

Perching

On the ESRP, several studies (e.g. Barraclough et al. 1967; Rightmire and Lewis 1987; Anderson and Lewis 1989) have shown that water episodically accumulates in perched layers that typically persist for a few months or years. While the layer contrast that allows perching to occur impedes vertical flow, the perched water itself is subject to rapid lateral flow, widening the influence of a localized water source. A broad area of perched water can facilitate access to aquifer-connected preferential flow paths, for example causing funneled flow (Kung 1990), facilitating transport to vertical fractures or other macropores, or generating fingered flow below a layer contact that causes perching. If the perched layer is sloped, there may be a significant vertical component of the enhanced flow within it.

Perching complicates hydraulic issues and contamination problems in several ways. The geometric complexity that perching introduces can lead to misinterpretation of hydrologic data (Davis 1994). Perching can be a critical element of runoff generation (Salve et al. 2012), though this may not occur when perched layers are at tens of meters depth. The reduced aeration within a perched zone may be a controlling influence on biochemical processes and it may become a zone of accumulation of contaminants. Monitoring of a perched zone can sometimes provide early warning of aquifer contamination.

The effect of perching on contaminant travel times has obvious importance. Other questions include what volume, thickness, and lateral extent of perched water body will develop for a given amount or rate of water inflow. Such

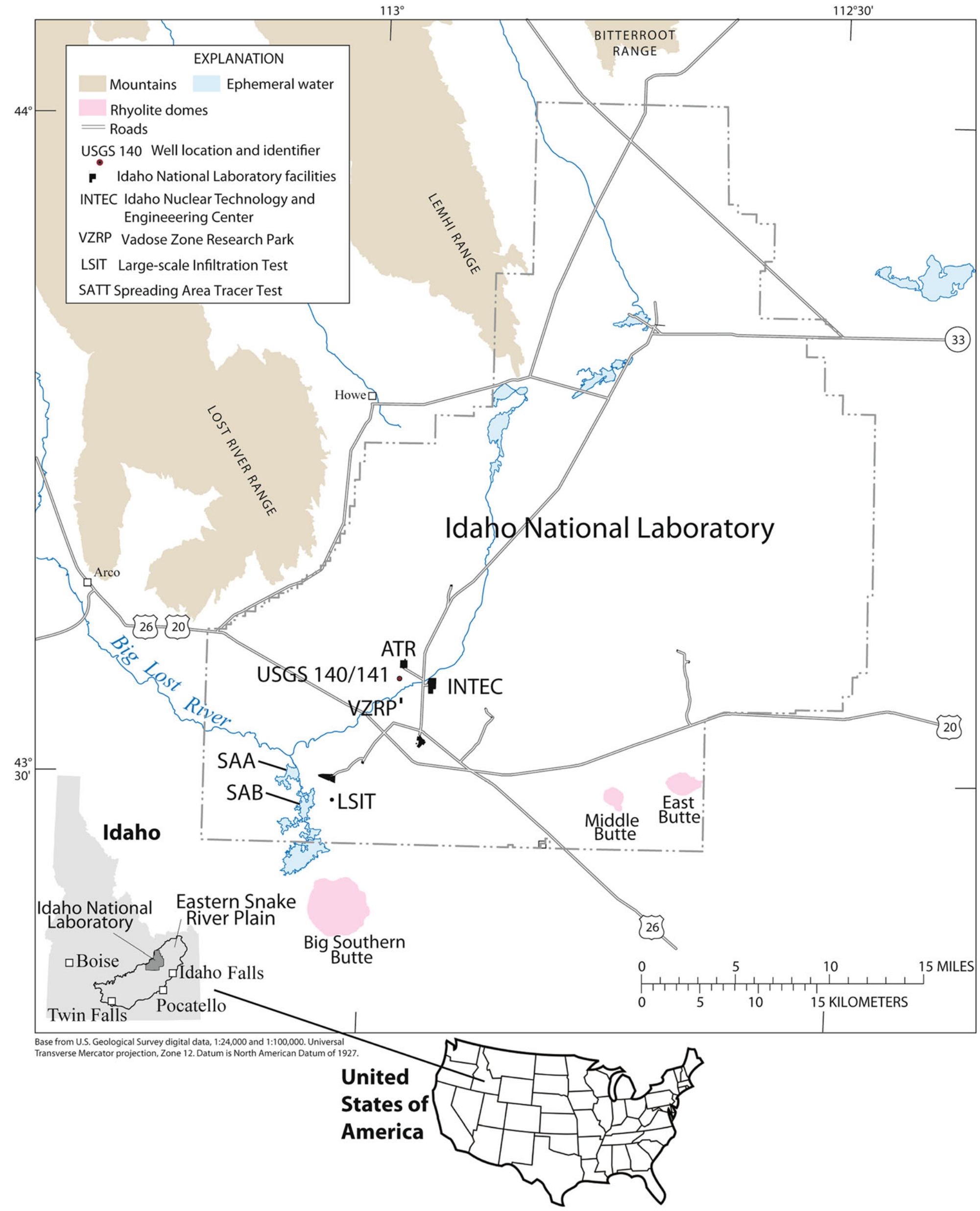

Fig. 1 The Idaho National Laboratory, Idaho, and selected facilities

geometrical issues are important for knowing how long perched water will persist, how broadly it will spread recharging water or contaminants from a localized source, and the likelihood of affecting an important subsurface feature such as a fault or a supply well. The lateral extent in particular is important to approach by theory or simulation, yet is poorly understood because, owing to the high cost of drilling the numerous test wells needed, few data are available (Robinson et al. 2005).

One straightforward approach to the quantification of perched water include is to solve Richards' equation for a stratified system in which the spatial variation of hydraulic properties determines where and how much perched water occurs (Hinds et al. 1999). A variation introduced by Robinson et al. (2005) includes flow impedances characteristic of the contacts between layers, as well as the properties of the layers themselves. Oostrom et al. (2013), in addition to a multiphase numerical approach based on transport properties of the subsurface materials, applied a Darcian scoping model that provides a simple relationship between perched water thickness, downward flux density, and properties of the layered materials. The model presented here is somewhat more complex than the scoping model of Oostrom et al. (2013), but much simpler than models based on multi-dimensional numerical solutions of partial differential equations of transport. It differs from other models also in incorporating explicitly distinct formulations for diffuse and preferential flow.

Objectives

The main emphasis in this paper is the subsurface hydraulic response to a major infiltration episode as could be caused by floods, ephemeral streamflows, artificial recharge, or periods of rapid snowmelt. The scope includes episodes in which nearly steady flow is established early enough that most of the input water moves through a substantial portion of the unsaturated zone during the time this condition holds. Though reducing applicability for short-duration events and advancing wetting fronts, this requirement permits attention to major infiltration episodes with great potential impact on recharge and contaminant transport.

Because models currently used for preferential and diffuse, variably saturated flow cannot simulate the types flow observed during tracer experiments (e.g. Nimmo et al. 2002; Dunnivant et al. 1998; Duke et al. 2007; Mirus et al. 2011), the development here includes a basic quantitative formulation of flow through the alternating sequence of materials. Predicted quantities include the thickness and areal extent of perched water bodies, and travel times to particular points in the subsurface. The model is developed for application in a forward mode, maximizing utilization of available hydrologic and geologic data, without heavy reliance on parameter calibration. After testing and refining the conceptual model using the best available parameter values, hypothetical scenarios and sensitivity analyses in response to plausible, major infiltration events are presented, taking the USGS 140/141 site as one example where the geology has been characterized but unsaturated zone hydraulics have not.

Approach

The many ESRP unsaturated-zone investigations since the 1950s, especially in and near the INL, have produced pertinent geologic and hydrodynamic information to understand some of the unsaturated zone flow behavior and estimate hydraulic property values. As at most sites, available unsaturated zone hydraulic property measurements lack the spatial resolution needed for representing all macroscopic heterogeneities. This deficiency motivates an approach that utilizes geologic data and quantifications in terms of effective properties that represent integral stratigraphic layers.

The model developed here uses data collected from some ESRP locations where both hydrodynamic and geologic data are available. The hydrodynamic data can facilitate direct estimation of the needed hydraulic properties. At others, some geologic data are available but unsaturated-zone hydrodynamic data are not, so it is useful to be able to predict hydraulic behavior from geologic knowledge. The unsaturated zone at USGS 140/141 has detailed geologic characterization data from two boreholes (Twining et al. 2014) and measured hydraulic properties of its sedimentary interbeds (Perkins et al. 2014), but no measurements that characterize the flow behavior of the basalt where preferential flow would be expected to occur under suitable high-flux conditions. For application to this and most other ESRP locations, a type of property-transfer approach is developed, based on data from locations where, in addition to lithologic characterization, there have been characterizations of the subsurface hydrodynamics associated with instances of substantial infiltration. Synthesized over broad regions of the ESRP, these data can facilitate predictive estimates of hydrodynamic quantities at locations where the unsaturated hydraulics have not yet been studied.

This work quantifies and interprets flow in sedimentary layers as diffuse flow based on Darcian formulations, in which flow rates are proportional to the driving force (i.e. hydraulic gradients). The proportionality constant, the hydraulic conductivity, is highly sensitive to conditions specified by state variables, particularly water content and matric pressure. Darcy's law is applied to both vertical and horizontal flow, in saturated and unsaturated conditions.

Preferential flow through fractured rock is quantified with source-responsive formulations (Nimmo 2010), in which the water flux applied to the system, rather than the usual state variables, largely determines the flow conditions. Based on generalizations of widespread observations, the source-responsive model quantifies preferential flow in relation to conceptually simple properties, with emphasis on the temporal distribution of water input. It augments the traditional Darcian theory for the diffuse component of unsaturated flow. Recent applications and developments of this model include: prediction of travel times (Nimmo 2007) and fluxes (Nimmo 2010), contaminant risk assessment (Ebel and Nimmo 2013; Mirus and Nimmo 2013), soil-water balance estimation of recharge (Cuthbert et al. 2013), prediction of irregular patterns of infiltrated water (Nimmo and Mitchell 2013), unsaturated-zone seasonal storage mechanisms (Nimmo and Malek-Mohammadi 2015), and incorporation into the VS2DT code for combined solution of Darcian and preferential unsaturated flow (Healy 2015).

Unsaturated zone of the Eastern Snake River Plain

The ESRP lies within a northeast-trending basin, approximately 320 km long and 80–110 km wide, which slopes gently to the southwest and is bordered on the northwest and southeast by the ends of northwest-trending mountain ranges (Fig. 1). The depth to the Eastern Snake River Plain aquifer ranges from 61 m in the northeast to 274 m in the southwest. The climate is semi-arid with 0.22 m average annual precipitation (US Department of Energy 1989), cold winters, little snowfall, hot dry summers, and high evapotranspiration.

Facilities and locations important to this study are shown in Fig. 1 and in the Appendix. These include the Vadose Zone

Research Park (VZRP), the site of the Large Scale Infiltration Test (LSIT), Spreading Areas A and B (SAA and SAB) used in the Spreading Area Tracer Test (SATT), the Idaho Nuclear Technology and Engineering Center (INTEC), the sampled boreholes USGS 140 and USGS 141, the Radioactive Waste Management Complex (RWMC), and the Advanced Test Reactor (ATR).

ESRP stratigraphy

Three classes of layers are essential to the model developed here. Their nature and basic hydraulic function are described in this section, with specific characterizing measurements summarized in the section 'Results'.

Surficial sediments

Toward the south, including the SAA, SAB, and LSIT sites (Fig. 1), the surficial sediments consist of well-developed silty soils. Farther north, including the VZRP and INTEC sites, at the surface are thick, poorly sorted alluvial deposits with pebble- to gravel-sized rocks. In general, the surficial sediment layer thickens to the north (Anderson et al. 1996b). Both preferential and diffuse flow through the surficial sediments have been observed (Nimmo and Perkins 2008).

Sedimentary interbeds

The sedimentary interbeds contain large amounts of sand, silt, and clay which, produced during quiet intervals between volcanic flows, are of fluvial, eolian, and lacustrine origin. Frequently the uppermost portion of an interbed is a baked zone, where a period of increased temperature during the deposition of hot lava irreversibly altered the chemical and structural properties of the sediments. Interbeds vary in thickness and continuity across the ESRP, ranging from less than 0.5 to more than 20 m thick. To the south, near the RWMC, seven main basalt flow groups and three sedimentary interbeds appear to be the most continuous (Anderson and Lewis 1989). The two interbeds of greatest thickness and continuity, and consequently greatest influence on water flow and perching, lie at approximately 33 and 73 m below land surface. To the north in the vicinity of the INTEC and ATR (Fig. 1), the sedimentary interbed structure becomes more complex as described by Anderson (1991) and Cecil et al. (1991). Along with the two main interbeds, numerous thin, discontinuous interbeds exist (Winfield 2003) that likely play a lesser role in water movement and perching. Interbeds tend to be denser than surficial sediments, and many are composed of lower conductivity silts and clays (Perkins and Nimmo 2000; Perkins 2003; Winfield 2003).

Basalt

Volcanic units, composed primarily of basalt flows, welded ash flows, and rhyolite, range from vesicular to massive with horizontal or vertical fracture patterns. The basalts extend as deep as 3,000 m below land surface and under the INL comprise about 85% of the subsurface volume to this depth (Anderson and Liszewski 1997).

Individual basalt layers, bounded above and below by sedimentary layers, typically are a few meters to tens of meters thick, and are generally composed of multiple basalt flows and flow lobes. The geometry of basalt flow lobes has been investigated in detail by Knutson et al. (1990) and Faybishenko et al. (2000), and summarized by others including Sorenson et al. (1996). The width of individual lobes is on the order of meters or tens of meters; vertical thickness is highly variable and typically much less than the width. Some thickness of the basalt immediately above a sedimentary interbed, which was subjected to rapidly changing thermal and moisture conditions during lava deposition, frequently constitutes a rubble zone, of high porosity with a gravelly or stony texture. Observations from closely spaced wells at the LSIT site (Fig. 2) indicate great heterogeneity in basalt layers, with individual lobes composed of various basalt types and rubble zones, greatly varying in density and fracture connectivity. Laterally, hydraulically significant heterogeneities (edges of lobes and their internal variations) are much more closely spaced in ESRP basalt layers, each composed of many lava flows, than in the sedimentary layers, which were formed through processes of greater areal uniformity.

Unsaturated zone investigations

Large-scale infiltration studies have been conducted at instrumented test sites on the ESRP. All of these show strong evidence of preferential flow and perching of infiltrated water. Perching in these studies occurred within and above a sedimentary interbed, typically the shallowest interbed in the profile that has substantial lateral continuity and hydraulic impedance. The Appendix provides diagrams, details, and results from these studies, which were used in the development and parameterization of the model.

Infiltration test sites

The four infiltration test sites used were:

1. *Vadose Zone Research Park (VZRP)*. At this site two infiltration basins were used to dispose of clean discharge water. Surficial sediments were approximately 20 m thick (Duke et al. 2007). The VZRP has extensive geologic and hydraulic characterization data from wells completed at both the surficial sediment-basalt contact and at the first

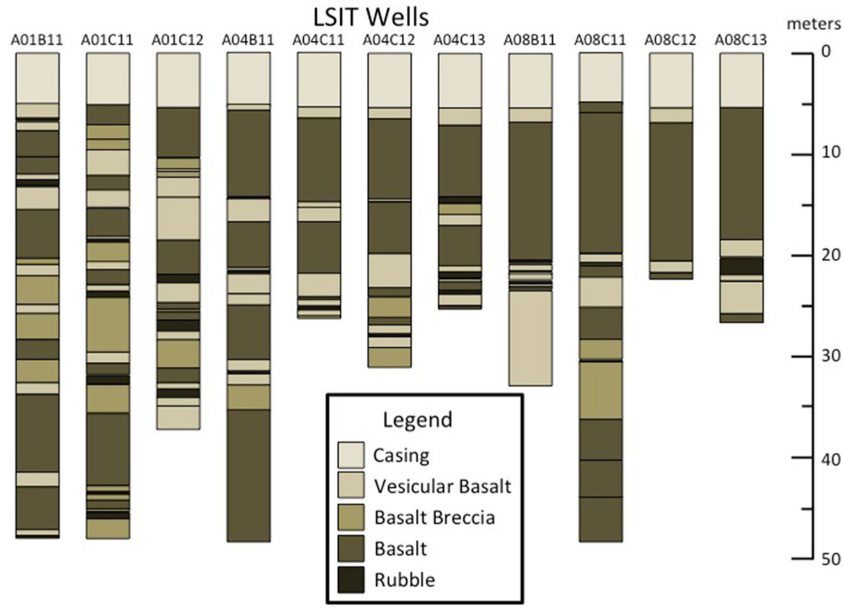

Fig. 2 Stratigraphy of wells within the LSIT basin. The three clusters *A01*, *A04*, and *A08*, each comprising closely spaced wells, are about 65 m apart

sedimentary interbed-basalt contact. The VZRP has been used to quantitatively observe and document the migration of water discharged into the ponds under mostly steady conditions, and from transient infiltration of the Big Lost River to the north of the park.

2. *Large-Scale Infiltration Test (LSIT)*. At the site of this field experiment, the surficial sediment layer was thin or absent, with a maximum thickness about 3.7 m and substantial basalt outcrops (Porro and Bishop 1995). Wood and Huang (2015) have presented a recent summary and interpretation of this field experiment. More than 60 instrumented monitoring wells were installed in and around a circular infiltration pond 183 m in diameter (Burgess 1995; Porro and Bishop 1995; Wood and Norrell 1996; Dunnivant et al. 1998). A high-volume pumping well maintained surface water in the pond for 36 days. Neutron probes, tensiometers, and geophysical instruments monitored water migration within the subsurface down to a major interbed at 55 m depth, both directly under the pond and in the surrounding area. Model development here assumes that surficial sediments extend to an average of 1.5 m deep, and that infiltration in effect goes directly into the basalts.
3. *Spreading Area Tracer Test (SATT)*. This field experiment made use of ponded water in SAA and SAB, southwest of the RWMC (Nimmo et al. 2002). The surficial sediments are thin and similar to those at the LSIT site. During the test in 1999, the spreading areas contained water diverted from the Big Lost River. This ephemeral river flows in early spring in years when there is enough snowmelt above Mackay dam, upstream of the ESRP, that management protocols dictate release of water from the reservoir. In 1999, Big Lost River flow was great enough to trigger intentional diversion to the spreading areas, used as infiltration basins. Tracer was added to the water in these areas and subsequently monitored using available wells.
4. *Idaho Nuclear Technology and Engineering Center (INTEC)*. The surficial sediments at the INTEC facility consist of gravelly alluvium, range from 2 to 20 m thick, and are thickest to the northwest (Anderson et al. 1996b), where the Big Lost River intersects the INTEC boundary. The subsurface is intensely instrumented with wells completed to various depths in the unsaturated zone and aquifer. Networked pipes at INTEC that convey clean water for fire-fighting purposes (called firewater) are monitored. In 2007, 2012, and 2013, instruments recorded perturbations of perched water level caused by three occurrences of firewater leaks. In this paper, these three occurrences are designated IL07, IL12, and IL13.

Geologically characterized test site

Though not having been investigated in infiltration studies, the otherwise well-characterized USGS 140/141 site is in the southwest portion of the INL east of the INTEC, north of the VZRP, and about 12 km northeast of the LSIT and SATT sites (Fig. 1). The surficial sediments extend to about 10 m deep (Twining et al. 2014).

Hydraulic behavior

Water perches above major layer boundaries as a result of infiltration from floods, snowmelt, and deliberate or accidental releases of water to the unsaturated zone. Artificial infiltration of wastewater has created perched zones that have persisted for several years (Orr 1999). Rubble zones, which often occur near layer contrasts where perching is likely, when effectively saturated, constitute an extremely conductive layer. The SATT showed that rapid downward flow, and substantial perching and lateral transport of water result from the infiltration of diverted river water in SAA and SAB. Water traveled through the 200-m unsaturated zone thickness in as little as 9 days, and laterally in perched zones approximately 1 km to wells at the RWMC and LIST. Cecil et al. (1991), with analysis of perched water levels in wells and water content profiles, showed that perching can take place within both sediments and basalts, and identified several causes. Specific mechanisms include (1) impedance of contrasts in vertical hydraulic conductivity between basalt flows and sedimentary interbeds, (2) reduced hydraulic conductivity in baked zones between basalt flows, (3) reduced vertical hydraulic conductivity in dense, unfractured basalt, and (4) reduced vertical hydraulic conductivity from sedimentary and chemical filling of fractures in basalt.

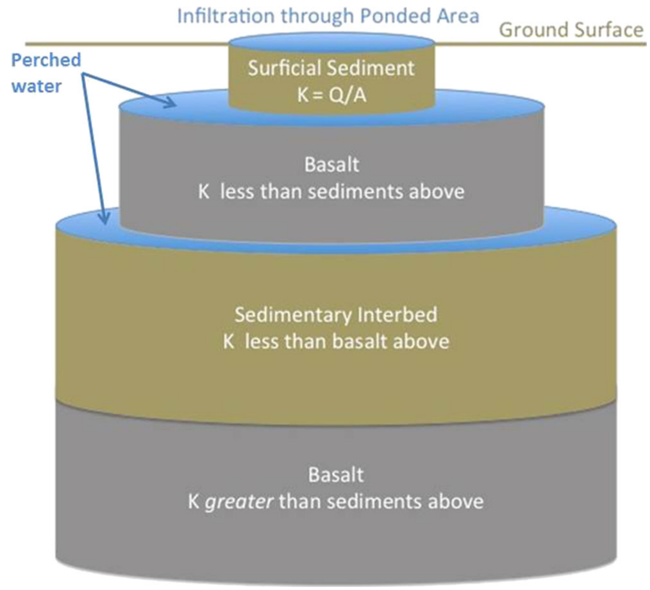

Fig. 4 Conceptual model with volumes of transmission represented as an idealized wedding-cake shape. The conceptual model applies as long as volumes of transmission are straight-sided; the cross-section does not have to be circular as pictured here

Theory and conceptual framework

Quantitative subsurface flow modeling relies on the conceptual model in Fig. 3, further idealized in Fig. 4. Infiltrating water moves through surficial sediments with varying degrees of spreading depending on the nature of the material. Water reaches the underlying heterogeneous basalt and flows mainly vertically in preferential paths down to the underlying, lower-conductivity interbed where perching and lateral spreading can occur. These processes recur as water reaches successively lower layers.

As mentioned in the previous, the formulations here apply to cases of effectively steady unsaturated zone flow in response to high-volume infiltration that continues for a sufficient length of time. The infiltration flux is of a magnitude that would be generated by shallow ponding. During the later portions of a major infiltration episode, the subsurface flow regime would approach a steady state through the unsaturated zone or to a given depth. For convenience, notation SSP refers to steady, surface-ponded conditions.

Much of this analysis is geared toward situations where the infiltration occurs over a limited area, entailing the possibility

Fig. 3 Conceptualized flow through the surficial sediments, heterogeneous basalt, and sedimentary interbeds that comprise the thick unsaturated zone of the Eastern Snake River Plain

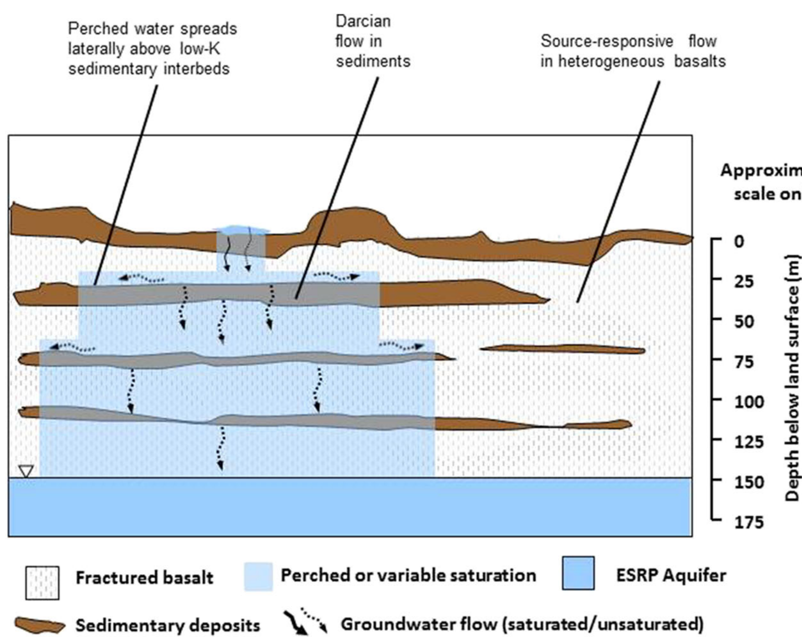

of significant lateral spreading within or between layers of the unsaturated zone. In this paper, *layer* refers to a depth interval of finite thickness whose composition allows it to be treated as a distinct unit characterized by a single set of effective hydraulic properties. Individual layers are indexed by subscript i, sequentially from the surface downward.

Although the distinction between flux and flux density is often neglected because a given study may deal entirely with one or the other, for the case of steady flow from a source of finite area into a stratified unsaturated zone, the distinction is essential. The symbol Q [L^3T^{-1}] stands for volumetric flux, the total volume of water passing through a hypothetical infinite plane per unit time, and the symbol q [LT^{-1}] for flux density, the volumetric flux per unit area of the plane through which it passes.

Diffuse flow

Diffuse unsaturated flow is assumed to follow Darcy's law, meaning that at a subsurface point with water content θ and steady flow driven solely by gravity, the downward flux density q numerically equals the unsaturated hydraulic conductivity $K(\theta)$ [LT^{-1}]. The value q_i entering layer i is determined by properties of the overlying layers. During steady percolation and SSP conditions, each layer has come to an effective average water content θ_i, at which its hydraulic conductivity $K(\theta_i)$ equals q_i according to the characteristic K–θ relation of the material, also referred to as the layer's effective hydraulic conductivity:

$$K_i = K(\theta_i) = q_i \tag{1}$$

For the surface layer, $K_i = K_1$ would also equal the infiltration capacity or infiltrability. Defining effective hydraulic conductivity in this way, which is appropriate only for steady flow, avoids the need to specify what θ value it corresponds to.

Preferential flow

The two main characterizations needed for source-responsive preferential flow are the medium's capacity for transmitting preferential flow (symbol M) and the degree of activation (symbol f) that represents how preferential flow will proceed with a given water input. Nimmo (2010) interpreted M [L^{-1}] as the inner facial surface area of potential preferential flow paths per unit volume. This does not equal the total facial area within all macropores or fractures, but only the portion that is subject to active preferential flow under conditions of maximal water input for the medium and location. The active area fraction f indicates the degree to which the available preferential flow paths are activated and connected, and varies from 0 when no preferential flow occurs to 1 when the preferential flow paths are completely activated. If the flux density into the top of the layer equals the value that ponding would generate if it were present above the layer, preferential flow would be maximal, implying $f = 1$. For lesser rates of percolation into the layer, which generate less preferential flow, $f < 1$.

At time t and vertical position z within the medium, the source-responsive flux density is

$$q_{\mathrm{sr}}(z,t) = V_{\mathrm{u}} L_{\mathrm{u}} M(z) f(z,t) \tag{2}$$

where V_u is a characteristic film-flow velocity and L_u the film thickness. In this formula, the film concept plays a role analogous to that of the capillary-tube concept in widely used unsaturated zone models for flow that is mediated by capillarity (e.g. Mualem 1976). The assumed geometric form of the flowing stream within the partially filled macropore links the water flux to a physical basis for its quantification. Preferential flow can occur in films of different thickness and flow velocity (Mirus and Nimmo 2013), as well as in other forms such as droplets and rivulets. Application to natural media is made with the understanding that the actual shapes of flowing streams are not uniformly thick films or perfectly cylindrical tubes. This paper's objective is not to modify this model but to utilize it, essentially as presented by Nimmo (2010), to represent preferential flow in fractured rock. The idealized film concept and the earlier V_u and L_u values of 8.6 m/day and 6 μm (Nimmo 2010; Mirus et al. 2011) are retained, giving 5.0×10^{-5} m^2/day (5.8×10^{-10} m^2/s) for the product $V_u L_u$.

Each basalt layer i, having preferential flow under SSP conditions, is represented by the effective macropore areal density M_{basalt} assumed for all ESRP basalt layers, and a particular effective active area fraction f_i. The flux density then is

$$q_i = V_{\mathrm{u}} L_{\mathrm{u}} M_{\mathrm{basalt}} f_i \tag{3}$$

which numerically equals K_i.

Unsaturated flow through multiple layers

For convenience of notation, for two layers in contact, index b designates the layer below (often the flow-limiting layer), and index a (= $b - 1$) the layer above (often the layer of perching).

Volumes of transmission

When the infiltration source is areally finite, an important quantity is the cross-sectional area through which the water is transmitted downward. In each layer water flows through a transmission volume, within which θ is elevated by newly infiltrated water. Because practical situations normally have few data to characterize the subsurface flow regime, this transmission volume needs to be represented by a simple shape requiring few parameters. This analysis takes the cross-sectional area of transmission A_i through the layer to be uniform (though not necessarily equal to the area of any perching below). The plausibility of this approximation is supported in basalts by direct observations from the LSIT, and in sedimentary layers by their typically modest thickness. This assumption of one-dimensional flow applies to the unsaturated portions of these layers, exclusive of perched zones, where the flow typically also has a strong lateral component. The shape of the cross-sectional area can in principle be an arbitrary closed curve in two dimensions, though particular cases may best be treated with a designated shape such as a circle.

Sequential source-responsive and Darcian flow

Each sedimentary layer, assuming Darcian flow, has a maximum effective hydraulic conductivity equal to the hydraulic conductivity at a field-saturated state, meaning the degree of saturation that develops from natural processes with a copious supply of water, as from flooding or high-intensity rainfall:

$$K_{\max} = K_{\mathrm{fs}} \tag{4}$$

The field-saturated state normally includes significant trapped air and other effects that make its hydraulic conductivity less than for a fully saturated state (Fayer and Hillel 1986). If q_i is large enough that θ_i comes to its field-saturated value, as for a layer that has ponded or perched water above it, the effective hydraulic conductivity K_i would equal the maximum value for the material of that layer (Eq. 4).

The artificial construct of effective hydraulic conductivity can also be applied to fractured rock layers undergoing source-responsive flow. As in the case of sedimentary layers, for SSP conditions, its value would equal the flux density under those conditions, but with that flux density determined by Eq. (3) rather than Darcy's law:

$$K_i = V_{\mathrm{u}} L_{\mathrm{u}} M_{\mathrm{basalt}} f_i \tag{5}$$

For a fractured rock layer under these conditions,

$$K_{\max} = V_{\mathrm{u}} L_{\mathrm{u}} M_{\mathrm{basalt}} \tag{6}$$

Use of this equivalence does not mean flow is Darcian within the fractured rock, but rather that the maximum flux density it can absorb without causing perching equals this maximum effective conductivity.

At a layer boundary, if the maximum hydraulic conductivity of the layer below, $K_{\max-b}$ is greater than or equal to q_a supplied to it by the layer above, the entire flux Q can proceed through the lower layer without a change in flux density, i.e. $q_b = q_a$. In the alternative case where $K_{\max-b}$ is less than q_a, $q_b = K_b$ if any perched head that develops in layer a is small compared to the thickness of layer b, written as

$$q_b = \min(q_a, K_{\max-b}) \tag{7}$$

where the function min(y,z) represents the lesser of its arguments y and z, and $K_{\max-b}$ is taken from Eqs. (4) or (6) as appropriate. If there is a layer j, typically the surface layer, where the flux density is known, another layer's flux density q_i can be determined by applying Eq. (7) repeatedly as necessary for the intervening layers. During steady flow, though the flux density can vary layer by layer if the areas A_i are unequal due to unequal K_i, the volumetric flux Q has a single value through the unsaturated zone, regardless of depth. The areas in different layers are related by

$$A_i = \frac{q_j}{q_i} A_j \tag{8}$$

which allows calculation of A_i for any layer in which q_i is known.

Conceptual model: stratigraphy

Within the surficial sediments, although the flow comprises both preferential and diffuse components, the flow is assumed to be primarily diffuse in character where this layer is thicker than about 3 m, as suggested by studies of the damping of post-infiltration moisture fluctuations. In the absence of detailed flow measurements, the layer's lower portions, compacted by substantial overburden and less likely to have preferential flow channels, are assumed to be the dominant control of flow that goes down to the next layer.

Diffuse flow is assumed to dominate the transport of water through the sedimentary interbeds, as it does through the deepest surficial sediments. Numerous core-sample measurements (McElroy and Hubbell 1990; Perkins and Nimmo 2000; Perkins 2003; Winfield 2003; Perkins et al. 2014) indicate wide variations of hydraulic conductivity and other properties within these layers. For model testing and flow prediction, effective hydraulic conductivity data were averaged from some of these laboratory measurements (Table 1). Within a sedimentary interbed, the lowest K sublayers likely dominate the perching and transport-rate processes of interest. These are likely to be fine-textured aeolian deposits. The general uniformity of depositional processes over time, as described in the preceding, gives reason to hypothesize that lateral and interbed-to-interbed variations in the limiting K value are modest.

Because of the pronounced lateral short-range (i.e. the approximate 10-m scale of a flow lobe) heterogeneity of any given basalt layer, it is inappropriate to treat it as a neatly stratified sequence of broadly homogeneous sub-layers. Instead, a basalt layer is characterized by effective hydraulic properties that apply through its whole thickness. Further, the sparse unsaturated-zone data available do not provide a basis for assigning distinct hydraulic properties to each basalt layer. Assuming that a consistent set of geologic processes created

Table 1 Typical characteristics of sedimentary layers, used in testing and predicting, at locations of interest in the ESRP

Location	Class of sedimentary material	Sediment character	Grain size: median [mean] (mm)	Effective K (m/day)	Water content (volumetric)	Reference: grain size	Reference: effective K
LSIT	Surficial	Silt loam soil with basalt outcrops	Not known	0.13	0.30	–	(Perkins and Nimmo 2009)
LSIT	Fine-textured interbed	Silt loam	0.017 [0.013]	0.015	0.45	(Perkins and Nimmo 2009)	(Perkins and Nimmo 2000)
LSIT	Sandy interbed	Fine to medium sand	0.315 [0.284]	0.13	0.45	(Perkins and Nimmo 2009)	(Perkins and Nimmo 2000)
VZRP	Surficial	Alluvial gravels mixed with silty and clayey sand	>4 [>4]	4.9	0.30	(Duke et al. 2007)	(Duke et al. 2007)
VZRP	Fine-textured interbed	Silt loam	0.058 [0.041]	0.047	0.45	(Perkins and Nimmo 2009)	(Winfield 2003)
VZRP	Sandy interbed	Fine to medium sand and gravel	0.304 [0.143]	0.13	0.45	(Perkins and Nimmo 2009)	(Winfield 2003)
SATT	Surficial	Silt loam soil with basalt outcrops	not known	0.79	0.42	–	(Barraclough et al. 1967)
SATT	Fine-textured interbed	Silt loam	0.017 [0.013]	0.025	0.45	(Perkins and Nimmo 2009)	(Perkins and Nimmo 2000)
SATT	Sandy interbed	Fine to medium sand	0.315 [0.284]	0.13	0.45	(Perkins and Nimmo 2009)	(Perkins and Nimmo 2000)
INTEC	Surficial	Alluvial gravels mixed with silty and clayey sand	>4 [>4]	4.9	0.30	(Duke et al. 2007)	(Duke et al. 2007)
INTEC	Fine-textured interbed	Silt loam	0.058 [0.041]	0.006	0.45	(Perkins and Nimmo 2009)	(Perkins 2003; Winfield 2003)
INTEC	Sandy interbed	Fine to medium sand and gravel	0.304 [0.143]	0.13	0.45	(Perkins and Nimmo 2009)	(Perkins 2003; Winfield 2003)
USGS 140/141	Surficial	Alluvial gravels and sand	>2	0.79	0.42	(Twining et al. 2014)	Similar to SATT
USGS 140/141	Fine-textured interbed	Silt loam	0.022 [0.040]	0.069	0.45	(Perkins et al. 2014)	(Perkins et al. 2014)
USGS 140/141	Sandy interbed	Gravelly sand and sandy loam	0.278 [0.121]	0.13	0.45	(Perkins et al. 2014)	(Perkins et al. 2014)

Volumetric water content and effective hydraulic conductivity are for conditions occurring during steady ponded infiltration. For the surficial sediments, effective K data are individual values from field infiltration experiments. For interbed sediments, effective K values are averaged from laboratory measurements on core samples. Perkins and Nimmo (2009) provided a summary of previously published measurements these basalt formations, a single set of effective hydraulic property values represents all ESRP basalt layers. This can be rationally conceptualized only in terms of a representative elementary volume (Bear 1972) of great lateral extent to encompass multiple basalt flows. Future investigations of water flow through the unsaturated fractured basalts could lead to refinements or locality-specific variations.

Several lines of evidence justify an assumed dominance of *unsaturated* preferential flow through the basalts of the unsaturated zone. The common occurrence of perched water in basalts normally extends upward only a short distance from the underlying interbed, such that the flow that supplies the perching goes through unsaturated conditions in the middle and upper portions of the basalt layer. Measurements of water content and matric potential within basalts during ponded infiltration experiments confirmed that unsaturated conditions dominate major portions of the basalt volume (e.g. Dunnivant et al. 1998; Faybishenko et al. 2000). The heterogeneity within a given basalt layer implies there are numerous instances where less conductive material overlies more conductive material. Gravity-driven flow in this system would ensure that unsaturated conditions persist at least in the most hydraulically conductive portions. The source-responsive model is appropriate for quantifying water flow in the basalts because much of it proceeds through fractures and other conduits that are only partially filled.

The LSIT provides evidence for the general prevalence of one-dimensional (at a scale of tens of meters) vertical flow through basalts. Based on neutron-probe measurements described in the Appendix, water content increased within the fractured basalt directly under the pond, but persisted unchanged at boreholes situated 15 m beyond the edge of the pond, except for a short depth interval immediately above the sedimentary interbed, where perching occurred (Porro and Bishop 1995; Dunnivant et al. 1998). This evidence suggests the water at this location did not spread significantly within the surficial sediments or the first basalt layer.

Conceptual model: integration

Considering flow from a surface source of finite area, the most idealized version of the conceptual model pictures the zones of transmission as a stacked set of concentric cylinders resembling a traditional wedding cake (Fig. 4). Equation (8) gives the cross-sectional area of the transmission zone in each layer as determined by fluxes and relative conductivities. Because the uppermost layer is at least several meters thick, whether basalt (LSIT site) or sediments (other locations), variations in ponded height above the land surface are assumed negligible in determining travel times. Where total flux Q is known but not area, as for injected water or subsurface leaks, with knowledge of effective hydraulic conductivity for the layer j where flow is introduced, equivalent effective ponded surface area A_j is estimated as Q/K_j.

At a restrictive layer i, an effectively saturated perched zone (likely including trapped air, at least initially) that forms above it, is assumed to supply the water percolating into layer i. This perched mound would likely be thinner near its edges, but for convenience is idealized as having uniform thickness H_i and area A_i, giving it volume $V_i = H_iA_i$. Note that H_i and V_i represent space within layer i–1, above layer i. If the mound is perched within the unsaturated zone, the height H_i is measured from the interface between layers i–1, and i. If the mound sits on a water table aquifer within layer i–1, H_i is measured from the level of the aquifer's water table.

The actual shape of the zones of transmission deviates from the highly symmetric picture in Fig. 4 for several reasons. These zones may be noncircular; assumptions and formulas concerning the area A_i do not require circular symmetry. In a real medium, inter-layer contacts will not be perfectly flat or horizontal. Layer-tilt will cause the transmission zones to be nonconcentric. These and other possible deviations must be kept in mind when applying this conceptual model to specific field situations, particularly when additional information may be available to constrain the shape of spreading zones (e.g. the strike and dip of an interbed). The Appendix provides further details from the various field studies that were used to inform the development of the conceptual model.

Perching phenomena

When the source of water can be approximated as uniform infiltration over an infinite plane, as for widespread rainfall or flooding over a large area, the basic relations between percolation flux densities and the fluctuating head of perched water can be formulated one-dimensionally (e.g. Heppner and Nimmo 2005; Nimmo 2010; Oostrom et al. 2013). Here, adaptations of these formulations are applied for the case where the source of water is an area of limited extent.

The water balance for the perched mound has two components, accretion by incoming water and depletion by downward flow through the limiting layer that causes perching. The incoming flux Q supplies a perched mound of volume V_a and uniform thickness H_a, necessarily $A_b = V_a/H_a$. For accretion occurring alone,

$$\frac{dH_a}{dt} = \frac{Q/A_b}{Y_a} \tag{9}$$

where Y_a is the effective specific yield within layer a, calculated as the difference in volumetric water content above and below the perched water table.

For depletion occurring through a sedimentary limiting layer, assuming that outflow from the mound moves downward according to Darcy's law driven by the head H_a,

$$\frac{dH_a}{dt} = -\frac{H_a}{\tau} \tag{10}$$

where τ is a time constant of exponential decline. The value of τ can be determined from fitting an exponential-decline curve to head-vs.-time data, $H_a(t)$. Examples of this sort of post-infiltration decline are shown in the Appendix. With accretion also occurring, the net water-balance is

$$\frac{dH_a}{dt} = \frac{Q/A_b}{Y_a} - \frac{H_a}{\tau} \tag{11}$$

Applying the geometric relation $V_a = A_b H_a$,

$$\frac{dV_a}{dt} = \frac{Q}{Y_a} - \frac{V_a}{\tau} \tag{12}$$

At steady state the mound volume is

$$V_a = \frac{Q\tau}{Y_a} \tag{13}$$

and the ponded height is

$$H_a = \frac{q_b \tau}{Y_a} \tag{14}$$

Where the effective hydraulic conductivity of a limiting layer is not known, it can be calculated from the dimensions of a steady-state perched mound that forms above it. The known geometry, in a rearrangement of Eq. (14), gives

$$q_b = \frac{H_a Y_a}{\tau} \tag{15}$$

Darcy's law gives this flux density as

$$q_b = -K_b \left[\frac{H_a + b_b}{b_b} \right] \tag{16}$$

where b_b is the thickness of the limiting layer b. The combination of Eqs. (15) and (16) indicates the effective hydraulic conductivity of the limiting layer:

$$K_b = \frac{H_a Y_a b_b}{\tau (H_a + b_b)} \tag{17}$$

in which all quantities on the right side can be estimated from measurements to give the value of K_b.

When the flow-limiting layer is fractured rock rather than sediments, and the flow is source-responsive rather than Darcian, Eq. (3) gives the flux density q_b. As long as there is some degree of perching at the top of that layer, as is normal when it acts as a flow-limiting layer, q_b is constant at its maximum value (i.e. $f = 1$) and equal to $K_{\max}$, given by Eq. (6). Combining with Eq. (15) and rearranging gives

$$M_{\text{basalt}} = \frac{H_a Y_a}{\tau V_u L_u} \tag{18}$$

This formula gives M_{basalt} from knowledge of the steady-state perched mound and its transient response to input cessation. In fractured rock layers that are not limiting flow, the effective active area fraction f_i can be determined by applying Eq. (3) during SSP conditions,

$$f_i = \frac{q_i}{V_u L_u M_{\text{basalt}}} \tag{19}$$

Travel times

Considering the travel time Δt_i through layer i as determined by advective transport, the travel time from the land surface to the bottom of layer k is

$$t_{0k} = \sum_{i=1}^{k} \Delta t_i \tag{20}$$

For source-responsive flow through layer i, the transport speed is just the standard value V_u (Nimmo 2010), so that

$$\Delta t_i = \frac{b_i}{V_u} \tag{21}$$

For diffuse flow, the application of Darcy's Law (Eq. 16) with the effective water content θ_i gives

$$\Delta t_i = \frac{b_i \theta_i}{q_i} = \frac{{b_i}^2 \theta_i}{K_i (b_i + H_{i-1})} \tag{22}$$

For sedimentary layers with diffuse flow that are not flow-limiting layers (not causing perching), or that cause perching of negligible thickness, this formula simplifies to

$$\Delta t_i = \frac{b_i \theta_i}{K_i} \tag{23}$$

Results

Effective hydraulic properties and flow behavior

For predictions, this model needs estimates of θ_i, and K_i for each diffuse-flow layer, and M_{basalt} and the specific yield Y_{basalt} for fractured rock layers. This section presents evidence for these, with more detailed information about the experiments and calculations given in the Appendix. Table 1 summarizes estimates of these for the sedimentary layers.

Surficial sediments

Thickness and coarseness of surficial sediments are correlated. Where the surface sediments are less than a few meters thick, they are soils that have developed from loess or lacustrine deposits. Where thicker, they are mainly gravelly alluvial deposits, coarser and more conductive. The increase in both layer thickness and typical grain size along an approximately SW–NE direction. This trend affects infiltrability, travel times, flow directionality (especially vertical vs. lateral), and perching behavior.

Where ponded infiltration has been measured, as for the LSIT, VZRP, and SATT, infiltrability tends to be greater for the more northeasterly sites. If material close to the land surface has a dominant influence on infiltration rate, this could explain the spatial trend. A thicker surficial layer could also contribute to the measured infiltration trend by affording a greater capacity for lateral spreading within the sediments. For infiltration and percolation over a finite area, enhanced lateral spreading in sediments would allow more infiltrated water to be accommodated above the normally less-conductive basalt. Such spreading varies from site to site. For the LSIT, with thin or absent surficial sediments, spreading was highly limited. At the VZRP, however, there can be significant spreading within the 20 m of surficial sediments. Infiltration pond data at the VZRP from Duke et al. (2007) suggests that water flowing through this layer of sediments can travel laterally at least 100 but less than 140 m before going through the underlying basalt.

Sedimentary interbeds

Sedimentary interbeds typically have numerous sublayers of various textures, from coarse sands and gravels to fine textured silts and clays, as shown by measurements of Perkins et al. (2014). Measured properties are available for relatively few of the ESRP interbeds. Therefore two effective values are used to represent two general classes of interbeds (coarse and fine).

Whereas the effective conductivity of coarse-textured layers within interbeds (0.13 m/day) is comparable to or greater than that of basalts, the effective conductivity of fine-textured layers tends to be significantly lower (about 0.03 m/day average). When diffuse flow dominates within the fine layers, therefore, these layers would limit the rate of downward flow through the unsaturated zone. These considerations, applied with the best available measured data, lead to the values listed in Table 1.

Fractured rock

Previous studies have shown that water moves quickly through the heterogeneous basalts, through gaps and fractures undergoing preferential rather than diffuse flow (Faybishenko et al. 2000; Nimmo et al. 2002; Duke et al. 2007). Data from the BLR-CH well at the INTEC show that the time lag between the initial flow in the Big Lost River and the initial response 150 m away at 40-m depth is 4–5 days (Mirus et al. 2011). Flow from anthropogenic leaks at the INTEC has similarly fast travel times, such as well responses after about 3 days at distances of 40 m and depths of 40 m (Forbes and Ansley 2008). Water at the VZRP has traveled 40 m vertically and about 100 m laterally in 2–3 days (Duke et al. 2007).

The LSIT provides a good case from which to estimate the macropore areal density M_{basalt} and the maximum percolation flux density (Eq. 6) for a basalt layer, because the ponded area had minimal surficial sediment and was large enough to incorporate much areal heterogeneity. The directness of the ponding on the basalt layer justifies setting $f = 1$ during SSP conditions, because the flux density from direct ponding is the highest that would occur over the range of land-surface conditions found on the ESRP. The average input flux Q was 3,500 m^3/day. Assuming the water percolating through this basalt layer stays within a transmission zone of area 27,000 m^2 (slightly larger than the 183-m-diameter pond), q_2 is 0.13 m/day and M_{basalt} using Eq. (3) is 2,600 m^{-1}. As explained concerning ESRP basalt characteristics in the site descriptions in the preceding, this value is assumed applicable to all basalt layers in the ESRP.

The rubble and the highly fractured vesicular rock of the basalt layers are likely to have specific yield comparable to that of the similarly constituted Snake River Plain aquifer. Lindholm (1996) summarized values of this specific yield ranging from 0.01 to 0.20. Here it is assigned the value 0.10, from the middle of this range. This value is comparable to expected porosities of this rock type, which can be estimated and corrected for trapped air using data collected by Marinas et al. (2013). If it is assumed that basalts have essentially zero water content when water is not flowing through them, the value of 0.10 also approximates the field-saturated water content, as would initially be achieved when perching begins.

Test cases

Predictions of the model developed in section 'Theory and conceptual framework' can be compared with measured travel times, depth of perched water, and lateral extent of perched water bodies.

Travel time through the unsaturated zone

The selected field infiltration studies provide tracer arrival times at the interbed immediately below the uppermost basalt layer, indicative of travel times through surficial sediments and a single thick layer of basalt. To compare them to predictions, therefore, would test only the source-responsive travel-time portion of the model (Nimmo 2007), producing little insight concerning ESRP hydrogeology. It is valuable, however, to consider the travel time through the whole sequence of layers down to the water table. One set of such measurements under SSP conditions is the tracer breakthrough curve from well USGS 120 during the Spreading Area Tracer Test (Nimmo et al. 2002).

Tracer for the SATT was added at the water surface after 21 days of ponding, when subsurface flow conditions were essentially steady. At USGS 120, completed in the aquifer at a depth of 205 m and located 100 m from the edge of the ponded body, tracer was detected in a transient spike 9 days after tracer application, and as a persistent breakthrough curve beginning 25 days after application (Fig. 5). The median tracer travel time was more than 100 days. For model comparisons the 25-day travel time is appropriate because (1) it applies to steady, not transient, conditions; (2) diffusion and dispersion are negligible for the short time intervals considered; and (3) the model specifically predicts first-arrival times (Nimmo 2007).

Neglecting the horizontal distance between the pond and the well, the predicted water travel times for each layer at USGS 120 are listed in Table 2, with some of their principal characterizing quantities. For basalt layers, the source-responsive advective travel velocity was taken to equal 13 m/days (Nimmo 2007). For sedimentary layers, the travel velocity was taken to equal the Darcian gravity-driven flux density divided by the estimated volumetric water content. The predicted sum of travel times is 14.6 days for the eight basalt layers and 117 days for the seven sedimentary layers. The total of 132 days is considerably larger than the 25 days from observations. Possible reasons for transport through sediments being faster than predicted, elaborated further in the discussion section, include preferential flow, inaccurate parameter values, and interbed discontinuities.

Thickness and lateral extent of perched zones

For the LSIT, the volume of the perched mound at steady state can be estimated from Eq. (13). For this calculation, the estimated the time constant τ is 14 days, based on regression to data from a period of recession after the infiltration had ceased. The calculated steady state volume of the mound within the uppermost basalt layer is 480,000 m^3. This value, divided by the area obtained using Eq. (8), establishes an estimate of perched thickness. With an effective specific yield of 0.10, the volume of added water within the mound would be 48,000 m^3.

At the VZRP, the water-transmitting area of surficial sediment-basalt contact and the mound volume on the interbed (layer 3) can be estimated using the value of M_{basalt}. The average Q discharged into the ponds during the VZRP test was 4,800 m^3/day. Using this flux and M_{basalt} = 2,600 m^{-1}, this transmission area is 35,000 m^2, equivalent to a circle of radius 110 m. This size falls within the range (100–140 m) that Duke et al. (2007) estimated for lateral spreading on the surficial sediment-basalt contact during the VZRP experiment. Regressing the recession data indicated τ of 4.2 days. Using Q_{in} = 4,800 m^3/days and a specific yield of 0.10, the predicted steady-state perched volume on the first interbed below the VZRP ponds (layer 3) is 200,000 m^3, the volume of the water itself being 20,000 m^3.

With a similar approach to other ESRP high-volume infiltration events, Fig. 6 compares the predicted and observed perched thickness. Observations are based on water levels in one or more wells, averaged where appropriate. Predictions for most of these infiltrations are in reasonable agreement. The poorest agreements are an overprediction for IL07 and an underprediction for IL12. The small input flux of these two events, markedly lower than the others, suggests the model's capability to predict perched water thickness is more reliable for events greater than a certain magnitude, perhaps a few hundred m^3/days, of input flux.

Figure 7 compares the predicted and observed areal extent of perched water. Each predicted value is the radius of the idealized circle having area calculated using Eq. (8). The observed minima are distances to the furthest well of detected perching, and the maxima, in two cases,

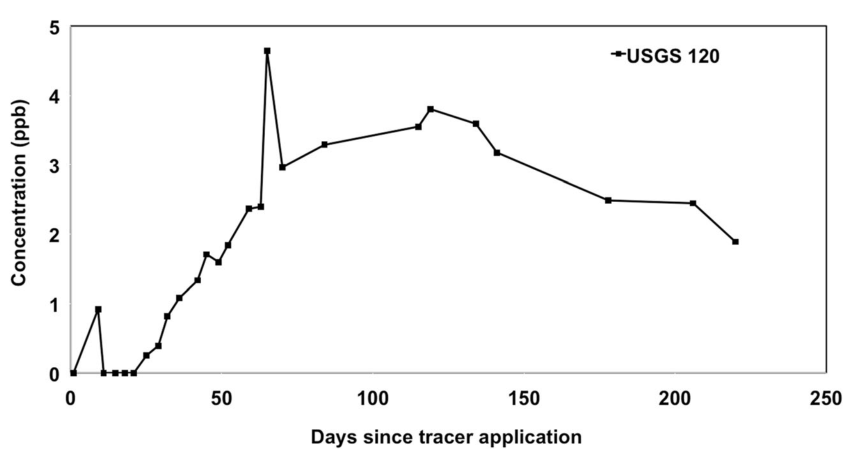

Fig. 5 Breakthrough curve of conservative tracer at aquifer well *USGS 120* during the SATT

Table 2 Predicted SSP travel times through the unsaturated zone at well USGS 120 for conditions of the SATT

Layer	Type	Thickness (m)	Predicted layer travel time (days)	Predicted cumulative travel time (days)
1	Surficial sediment	3.7	1.9	2
2	Basalt	36.3	2.8	5
3	Sandy interbed	6.1	21.1	25
4	Fine interbed	6.1	39.8	66
5	Basalt	24.7	1.9	68
6	Fine interbed	4.3	27.8	95
7	Basalt	4.0	0.3	96
8	Fine interbed	2.7	17.9	114
9	Basalt	35.7	2.7	116
10	Basalt	64.6	5.0	121
11	Fine Interbed	1.2	4.2	125
12	Basalt	7.9	0.6	126
13	Fine interbed	1.2	4.2	130
14	Basalt	9.8	0.8	131
15	Basalt	6.7	0.5	132

Water contents and effective K values used in calculating travel times are taken from Table 1 for the corresponding layer type. Stratigraphic data here are from Anderson et al. (1996a)

are distances to the nearest tested well with no observed perching. Irregularity and slope of the layer topography add to the uncertainty, but because the extent in any given direction from the center of the infiltration source may be greater or less than the radius of the circle, this assumption does not necessarily create a bias toward greater or lesser values.

Water balance

In cases where it is known which layers contain infiltrated water, an estimate of the volume of infiltrated water within the unsaturated zone can be calculated from the mound thickness and spreading calculations. The layers holding resident infiltrated water can be identified from the duration of water input and the travel times through the basalts and sediments. For basalt layer i containing perched water, the volume of infiltrated water within the mound is

$$V_{wi} = H_i A_i Y_i \quad (24)$$

For sedimentary layer j containing perched water, the volume of infiltrated water within it is

$$V_{wj} = b_j A_j \Delta\theta_i \quad (25)$$

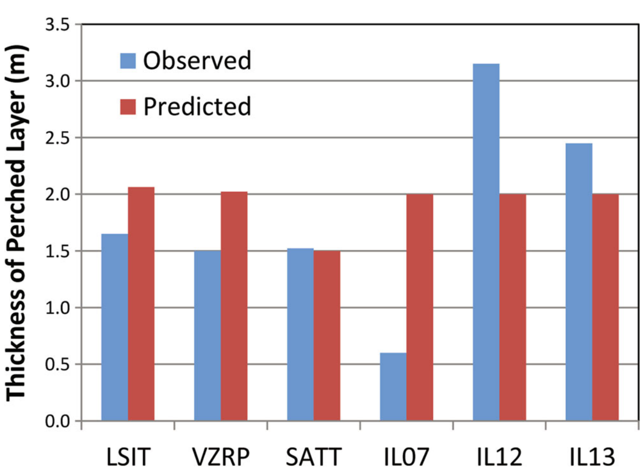

Fig. 6 Predicted (*red*) perched thickness, compared with observed (*blue*) values, in several ESRP investigations of high-volume infiltration

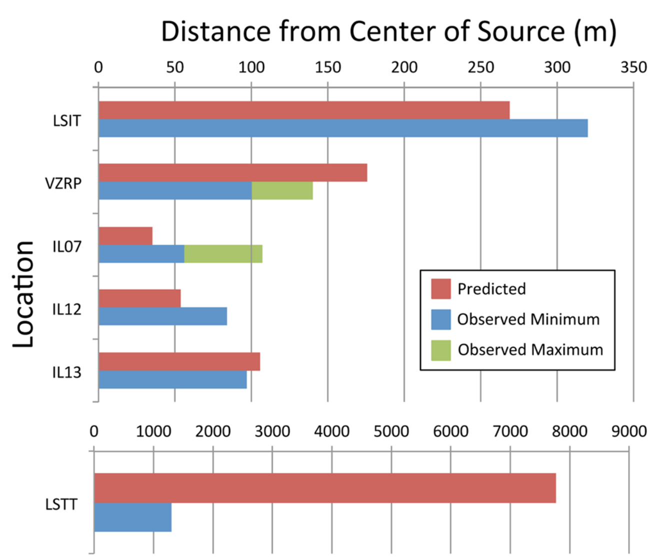

Fig. 7 Predicted distance of lateral spreading (effective equivalent radius) of perched layer in several ESRP investigations of high-volume infiltration

where b_j is the layer thickness and $\Delta\theta_j$ is the difference between the final and initial water content. Summation of these volumes for the layers with infiltrated water gives the volume of water added to the unsaturated zone

If the duration of infiltration is short enough that the amount of infiltrated water added to the saturated zone is modest, the total added water in the unsaturated zone may approximately equal the total contribution to infiltration. The LSIT experiment and three INTEC leaks appear to meet this criterion. Table 3 compares the total volume calculated from the modeled spread and thickness within the unsaturated zone with the volume known from the input rate and duration. Although for the INTEC 2013 leak the calculation overestimates by a factor of 6.5, the generally fair agreement suggests the calculations of volume based on spreading and thickness are reasonable.

Model-predicted subsurface behavior at the USGS 140/141 site

Lithology

Having tested the model's ability to estimate hydrologically important information such as travel times and spreading distances, this section illustrates its application in a predictive mode. Figure 8 illustrates the observed lithology at wells USGS 140 and USGS 141 (Twining et al. 2014). Surficial sediments extend 10.4 m deep at USGS 140 and 11.6 m deep at USGS 141. The stratigraphy over the 100-m distance between these wells, compared to wells in other ESRP locations, is more continuous. The thickness of the surficial sediments is fairly uniform—10.4 m at USGS 140 and 11.6 m at USGS 141. There are fewer distinct interbeds than at other ERSP locations; four interbeds appear in USGS 140 and five in USGS 141. The surficial sediments and the first 2 interbeds exhibit a slight change in thickness and relatively flat average slope over the 115-m distance between the wells. The deepest interbed (the fifth in USGS 141, 154 m below the surface), because it appears in only one of the wells, is clearly not continuous in this area. The four other interbeds appear to be laterally correlated. Having greater apparent slope, the third and fourth interbeds could promote stronger lateral movement of water perched on them.

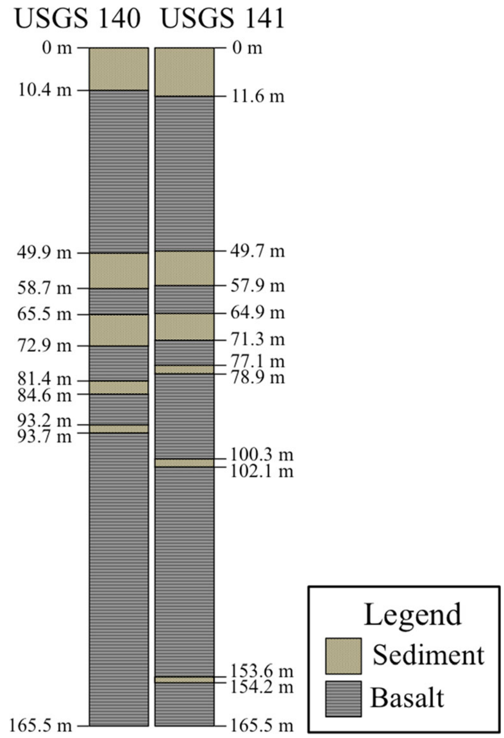

Fig. 8 Stratigraphy of the two wells near the USGS 140/141 site

Table 3 Comparison between volumes of infiltrated water from measured inflow to the infiltration source, and estimated through model calculations of spreading, thickness, and travel time

Event	Total volume estimated by model calculations (m^3)	Total volume of measured inflow (m^3)
LSIT	1.41×10^5	1.33×10^5
IL07	6.40×10^3	5.70×10^3
IL12	1.78×10^4	7.40×10^3
IL13	8.43×10^4	1.29×10^4

Model predictions

Knowledge of the stratigraphy at the USGS 140/141 location facilitates estimation of subsurface hydraulic response to major infiltration episodes. Illustrative modeled responses are computed assuming, for comparability to a flood response, an infiltration rate of 0.79 m/day (Table 1). Calculating the travel time with the same assumed layer properties used for other sites, the model predicts the infiltrated water would take 360 days to reach the aquifer, having 10 days of travel time through basalt and 350 days through sediments (Table 4). This travel time is likely overestimated, as noted above, because the simple Darcian calculation of flow through sediments is likely inadequate for this purpose, especially when interbeds are discontinuous or leaky.

Perched mound estimates were computed at the first interbed (Table 5). Given flow rates of 55, 263, 3,500, and 4,740,000 m^3/days (corresponding to observed values for IL12, IL13, LSIT, and SATT, respectively), the area of spreading at land surface, perched water thickness, and lateral extent of perching were estimated. The area at land surface scales with flow rate. The perched thickness depends only on the value of τ for this location. In the absence of perching data, τ is given the average value, 14 days, of τ values from the four

Table 4 Predicted SSP travel times through the unsaturated zone at the location of well USGS 140

Layer	Type	Thickness (m)	Water content (-)	Predicted layer travel time (days)	Predicted cumulative travel time (days)
1	Surficial sediment	15	0.42	8.0	8.0
2	Basalt	39	–	3.0	11
4	Fine interbed	8.0	0.45	52	63
5	Basalt	7.0	–	0.5	64
6	Fine interbed	7.0	0.45	45.7	109
7	Basalt	7.0	–	0.5	110
8	Fine interbed	3	0.45	19.6	129
9	Basalt	15	–	1.2	131
10	Fine interbed	1	0.45	6.5	137
11	Basalt	68	–	5.2	142

sites in the ESRP (14 days for LSIT, 4.2 days for VZRP, 6.0 days for SATT, and 33 days for INTEC) where there are perching data. Independence of perched thickness from input rate results from the limitation on flux density imposed by the basalt layer above the interbed; if flow through the transmission area in the surficial sediments exceeds the maximum flux density of the basalt, the infiltrating water would spread laterally above the interbed and cover a greater area, rather than increasing the vertical accumulation. This same mechanism causes lateral travel distances to increase with flow rate.

Sensitivities

The simplicity of the model's formulation facilitates the evaluation of sensitivities to subsurface characteristics. Perched thickness is proportional to τ, a range of about a factor of 8 over the sites investigated. The lateral extent is slightly more complicated, having a square-root relationship with conductivity. This sublinear dependence moderates the increase in lateral extent that comes with greater input flux or lower conductivity of the layer that causes perching. Travel times vary considerably with the dominance of preferential vs. diffuse flow modes, so the overall proportions of basalt and sediment likely have great effect.

Table 5 Predicted perched water thickness atop interbed, and lateral travel distance at the USGS 140/141 site, given a range of selected steady-state flow rates and corresponding ponded areas at the land surface

Analog event for input flux	IL12	IL13	LSIT	SATT
Input flux at surface (m^3/day)	55	263	3,500	4,740,000
Area at land surface (m^2)	69	333	4,430	6,000,000
Perched thickness (m)	3.5	3.5	3.5	3.5
Lateral travel distance (m)	26	56	211	7,769

Discussion

Model purpose and design

For major inputs of water such as prolonged flood infiltration, into thick geologically complex unsaturated zones, the model developed here estimates important hydrologic variables including vertical travel times, occurrence of perched water at layer interfaces, and the volume and extent of perched water. The ability to make direct, forward-model predictions of these quantities is possible in part because the model is limited to steady-state conditions in response to a substantial input of water to a finite area of the land surface. This condition tailors the model to applications related to natural and artificial ponding, flooding, or substantial water release, which have critical importance to aquifer recharge and contaminant transport. It applies not to the early stages, but to the later, effectively steady portion of major infiltration events, when the potential for fast, high-volume transport is greatest. This model addresses coupled diffuse and preferential flow processes that are of concern in thick, stratified unsaturated zones. Important features underlying the model include preferential source-responsive flow in fractured rock, diffuse Darcian flow in sediments, and the development of perched water at layer boundaries where an incoming flux density exceed the lower layer's effective conductivity. Required inputs for fractured rock layers concern the abundance of preferential flow paths and the fraction of those flow paths that are active. The main required input for sedimentary layers is the effective conductivity that occurs when the response to ongoing infiltration has become steady.

For characterization of the subsurface, the implementation of this model in the ESRP utilizes a large body of observational evidence from hydrogeologic field experiments and measured natural conditions, further described in the Appendix. For the preferential flow in fractured rock, based on currently available hydrodynamic data from the ESRP, it is not justifiable to use a more detailed representation of the source-responsive M parameter than a single value (2,600 m^{-1}) computed from observed conditions. Available observations suggest that surficial sediments are more conductive than the basalt layers. The common observation of perched water within and above sedimentary interbeds indicates that at least some of these interbeds are less conductive than the basalt layers.

The typical deficiency of hydraulic-property knowledge motivates not only a simplified model but also a property-transfer approach, in which hydraulic properties at the location of interest are based on those of one or more related locations, adjusted appropriately for locally observed characteristics. Diverse types of information are useful for this, for example characteristics of the geologic framework; measured travel times from tracer experiments, core-sample measurements of hydraulic properties; and observations of perching, especially in terms of heads, lateral extent, and persistence.

Tests and applications

Predictions with this model can be produced deterministically, as the test cases demonstrate for travel times and perching behavior. The source-responsive modeling of travel times give results comparable to observation when the flow is through basalt layers, even though, as discussed in the following with model limitations, the Darcian calculation of flow through sedimentary layers sometimes does not. The model can predict the thickness of a perched zone above a layer boundary, in accord with the incoming and outgoing water balance. The perched water body evolves toward a thickness and areal extent dictated by (1) the incoming flow of water from above, and (2) the downward percolation into the layer below, which cannot exceed that layer's maximum hydraulic conductivity. This calculation relies heavily on knowledge of the effective K of the underlying layer, for which a useful information source is the measured perched-water decline rates after cessation of inflow to the perched zone. The lateral extent of perching is sensitive primarily to the effective hydraulic conductivity of the underlying layer in comparison to the incoming flux density at the level of perching. For this quantity, important to contaminant transport and artificial-recharge applications, few observations are available because there are few suitable wells.

The model predictions of thickness and extent compare well with observations, but agreement of travel times is poor, as indicated by predictions of SATT tracer travel times at USGS 120 (Nimmo et al. 2002). An important inference is that interbeds have greater effect for perching than for retardation of advective transport. Possible reasons for the model's overestimation include firstly that some form of preferential flow may occur through most sedimentary layers, so that the Darcian calculation is inappropriate for this purpose. Preferential flow is well known to occur in the surficial sediments (e.g. Nimmo and Perkins 2008) and may also occur in interbeds. Secondly, the parameter values for fine interbeds (Table 1) may have the effective hydraulic conductivity too low or water content too high, either of which would overestimate travel times. This possibility is unlikely to be the main reason, however, because these values are based primarily on unusually accurate core-sample measurements. Thirdly, discontinuities in the interbeds may be common enough that water-transporting pathways through basalt bypass most interbeds. Little is known about subsurface features that would permit such bypass because of the limitations and high cost of subsurface characterization methods. More detailed knowledge of interbed continuity, uniformity, topographic variations, and heterogeneity is needed for comprehensive travel-time prediction. For present applications, better predictions would be obtained by assuming that vertical flow down to the water table is preferential as if determined entirely by the fractured rock. Travel times, especially for first arrival, may be more accurately predicted by assuming interbeds have either gaps or vertical preferential flow paths that circumvent the retarding effect of Darcian flow.

Simplifications and limitations

Some model simplifications include:

1. *Geologic features are idealized as being horizontal and uniformly thick*. Realistic topography, at short range, has ridges, bumps, and depressions that guide perched water to an irregular pattern of spread; these also may focus flow into the next layer. At longer ranges, any significant net slope of a layer interface will bias the lateral flow direction of any perched water at that interface.
2. *The use of lumped effective properties to represent stratigraphic layers*. Fractured basalts have substantial lateral heterogeneity at scales of a few meters or less, smaller than typical layer thickness. Surficial sediments vary less at this scale, but are strongly variable over much larger lateral distances; they have fewer geological processes in common, across distances, than basalts or interbeds. Spatial variability also results from additional location-specific influences such as weather and vegetation patterns. Interbeds, on the other hand, are less subject to these sorts of effects, and also are subject to additional processes that may decrease spatial variability, such as high overburden pressures, baking while lava is flowing, and absence of much flora and fauna.
3. *Neglect of lateral flow other than spreading of perched water*. In addition to gravity, capillarity can drive unsaturated flow, without the downward bias of gravity. High-

flow events may in general be dominated by gravitational flow and lateral spreading due to effective conductivity contrasts, but in thick or fine sedimentary layers lateral capillarity-driven flow may be significant

These simplifications are comparable to those normally used in hydrogeologic modeling at intermediate to large scales. Besides creating quantitative uncertainty, their use entails the danger that critical processes may be neglected—for example those deriving from system heterogeneity. Despite unavoidable simplifications, however, the model results can provide a particularized understanding of local hydrologic phenomena based on the most advanced science available, producing insights useful for management and monitoring purposes related to recharge and contaminant containment or mitigation.

Further development and broader application

Additional applications would become possible with development that extends this model to the transient case. An obvious example is the prediction of early-stage travel times and lateral travel times in perched layers, important for events of relatively short duration. Such an extension would also allow estimations of the time and conditions required to establish steadiness.

This model can be applied to locations other than the ESRP with modest data requirements. The main requirement for applicability is an unsaturated zone with contrasting layers, as needed to cause perching of water at layer boundaries. The model's most important use would likely be in situations where some, but not necessarily all, layers transmit preferential flow. Some of the needed site-specific properties could be characterized by local measurements or by property transfer from the ESRP or more closely related sites.

Conclusions

For one extensive area of interest, the ESRP, using results from several previous unsaturated zone investigations, this study has inferred the properties needed to quantify and predict preferential flow in unsaturated zone fractured rock, diffuse flow in sedimentary layers, and the thickness and areal extent of perched water bodies.

Synthesis of data and observations from several major field experiments gives insight into hydrologic processes at the ESRP. Available knowledge of ESRP unsaturated zone materials suggests that surficial sediments are in general the most conductive and also the most spatially heterogeneous. They strongly influence the flow below. Basalts are less conductive than surficial sediments but more conductive than some, perhaps most, interbeds; the common observation of perched water within and above sedimentary interbeds indicates that at least some fraction of the interbeds are less conductive than the basalt layers.

This investigation has developed an advanced capability for predicting subsurface hydraulic response to a specific, hydrologically important type of event, namely, a large input of water over a finite area of land surface that continues long enough to establish steady conditions in the unsaturated zone. It does so with a combination of simple formulations, namely, diffuse flow by standard Darcian techniques and preferential flow by the source-responsive model. It provides a quantitative description of flow through alternating sedimentary and fractured-rock materials, including cross-sectional areas of flow transmission and generation of perched water. The main predicted quantities are vertical travel times, the thickness of perched layers, the lateral extent of perched water, and the volumes of infiltrated water contained within individual unsaturated-zone layers. With this modeling approach it is possible to predict important features of unsaturated zone flow resulting from hypothetical scenarios, based on property transfer to a location with available geologic, but not necessarily hydrologic, characterizing information.

Acknowledgements This work was funded in part by the USGS INL Project Office. The authors are grateful to those who provided data and background information, including especially Jeff Forbes of the Idaho Cleanup Project and Tom Wood of the University of Idaho. Annette Schafer, of Battelle Energy Alliance, and several other reviewers and editors improved the quality of this paper.

Appendix: Evidence to support the conceptual model

This study relies strongly on data from infiltration experiments conducted at four particular ESRP locations, designated LSIT, SATT, VZRP, and INTEC (Fig. 9). This Appendix gives details concerning three of these.

LSIT

The Large Scale Infiltration Test was conducted in 1994 (Wood and Norrell 1996). A circular pond, area 26,300 m^2, was filled with water at a constant head for 5 days, allowed to drain for 11 days, and maintained at a constant head (maximum 1.4 m) for 19 more days. Water remained in the pond at declining level for 11 more days after replenishment had stopped.

Sixty-six instrumented wells within and around the pond were used to monitor flow through basalt and perching on top of the sedimentary interbed at 55 m depth. The wells were arranged in four rings, designated A, B, C, and E, in order of increasing radii (Table 6). The wells were grouped in clusters, usually of three, positioned at approximately equal

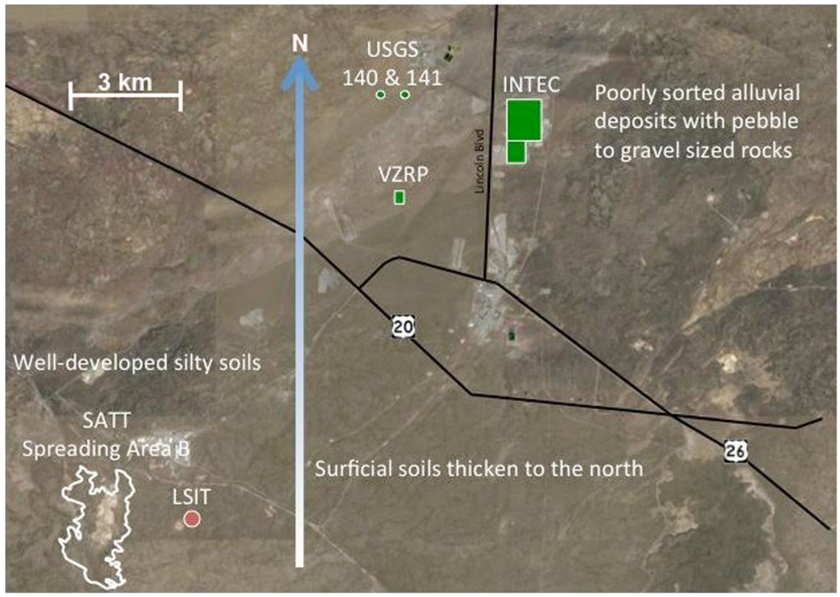

Fig. 9 Sites of major surface infiltration experiments on the ESRP, noting the spatially varying trend of surficial sediment characteristics

spacing around the circumference of each ring. Within each cluster, except one in the A-ring, one well was drilled to the interbed and the others to shallower depths. Two wells were drilled through the interbed.

To evaluate changes in water content above the first interbed, neutron counts over a range of depths in the wells were measured daily from June 23 until the end of August 1994. The data from A wells (within the pond) show an increase in water content during the period of ponding (Fig. 10a). Data from the B wells, however, show no increase in water content (Fig. 10b). This suggests that infiltrated water in the surficial sediments or in the basalt did not migrate laterally more than 15 m beyond the edge of the pond, where the B wells are located.

Water from the pond began infiltrating when the experiment started on July 25, 1994, and perched water was first detected on August 8. Results from the measurements are plotted in Fig. 11. The A wells reported much higher perched water elevations than the B, C, or E wells and show no rising or falling limb because these wells were completed at levels considerably above the interbed.

Table 6 Radial layout of LSIT site

Radius from pond center (m)	Notable feature
46	4 A-well clusters
91.5	Edge of pond
107	10 B-well clusters
183	8 C-well clusters
320	4 E-well clusters

The A wells show no trend in perched water-table elevation over time. The B wells do exhibit a trend over time, all but two of them (B08N11 and B09N11) reaching elevations of 1,492.0 to 1,492.5 m. The two exceptions are considerably lower than the rest, possibly because of a topographical impediment that limits the flow to these positions. The elevation of perched water in the C wells is lower than that in the B wells, and in the E well is less than any others. This trend suggests that the perched water elevations decrease with distance from the infiltration basin (Porro and Bishop 1995).

VZRP

During the 2007 VZRP experiments, the average rate of water discharged into the ponds was 4,800 m^3/day. Though the pond basins at the surface were larger, actual ponded water during these experiments never covered an area larger than about 1,000 m^2. Data from Duke et al. (2007) suggest that infiltrated water spread laterally within the relatively thick (15 m) VZRP surficial sediment layer before flowing into the underlying basalt. The data indicated this spreading extended laterally at least 100 m, but no more than 140 m. The area of percolation into basalt then was between 31,400 and 90,800 m^2, much larger than the ponded area at the surface.

INTEC leaks

Two wells at the INTEC facility, MW-6 and 33-3, exhibit significant responses to nearby anthropogenic leaks of water intended for fire-fighting (Fig. 12; Forbes and

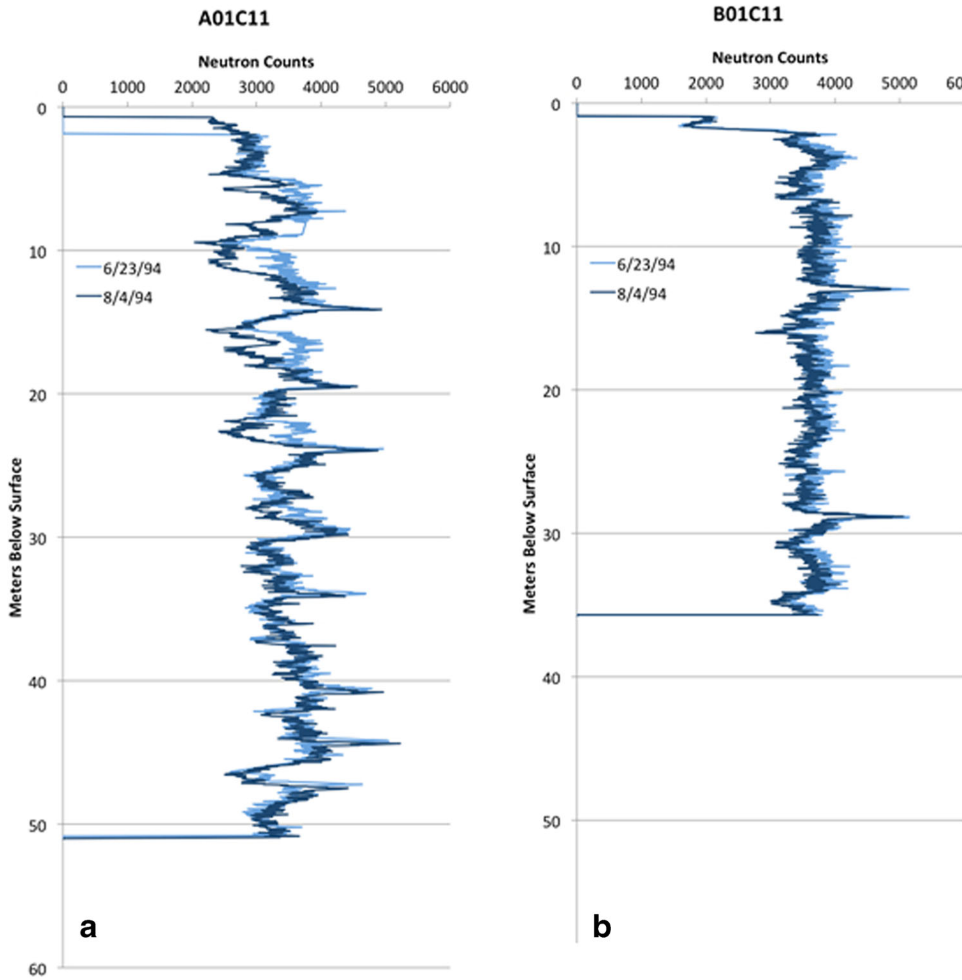

Fig. 10 Neutron counts before the experiment on June 23, 1994, and during the experiment on August 4, 1994: **a** well A01C11 within the pond radius, and **b** well B01C11 outside. More counts indicate less water, so water content increases to the left

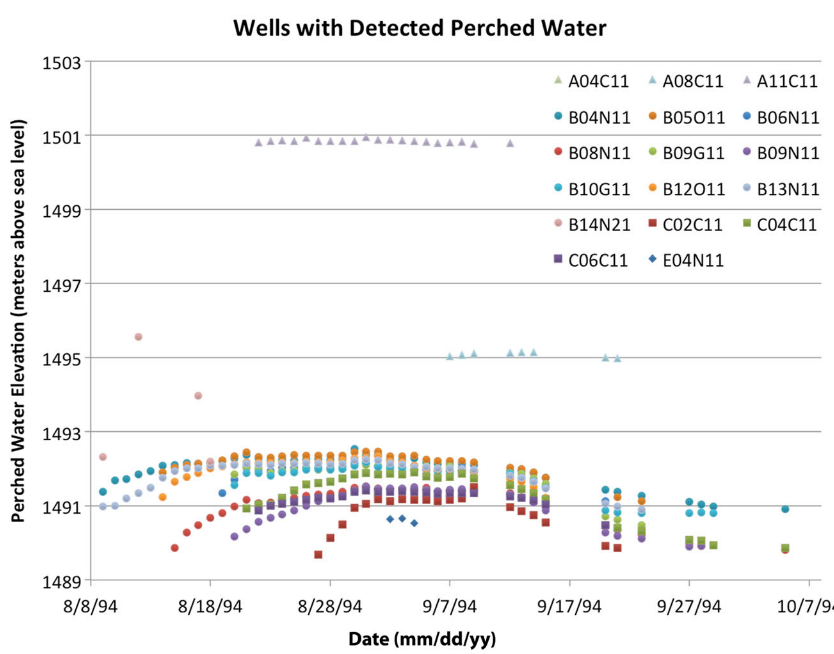

Fig. 11 Perched water-table hydrograph for all wells with perched water detected during the LSIT

Fig. 12 Aerial view of wells *MW-6* and *33-3* and three leaks at the INTEC facility

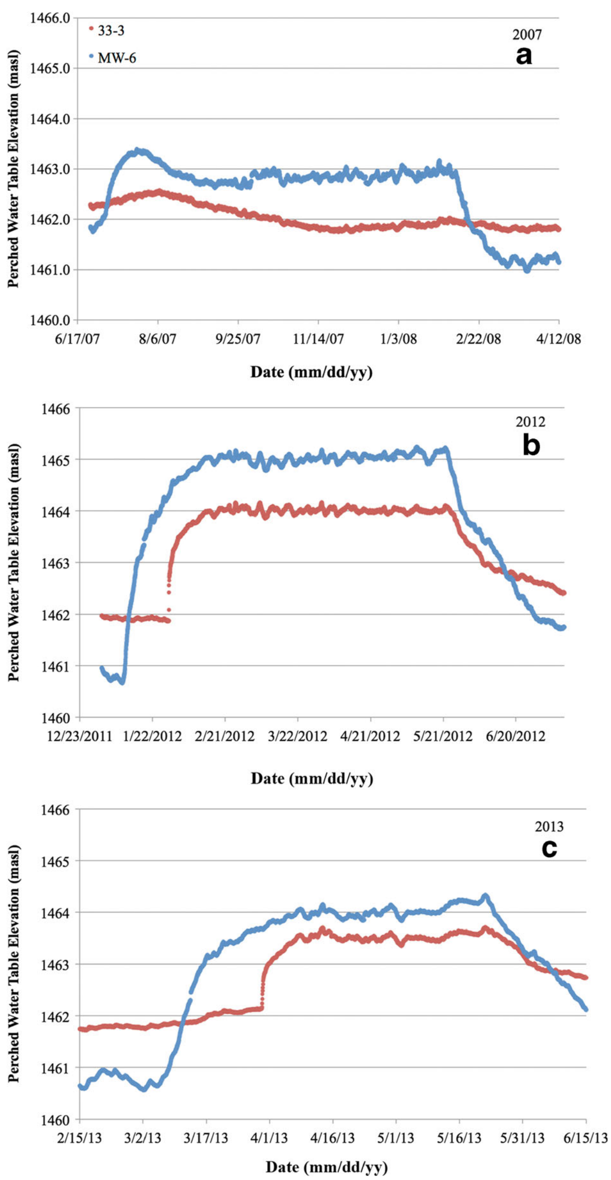

Fig. 13 Perched water table hydrographs for wells *33-3* and *MW-6* during near-surface water leaks at INTEC in **a** 2007, **b** 2012, and **c** 2013

Ansley 2008); J. Forbes, Idaho Cleanup Project, personal communication, 2014). Figure 13 shows the hydrographs of these wells.

The first leak, from fire hydrant HYD-0521, began leaking on June 27, 2007, and was stopped on February 6, 2008, after releasing an estimated 5,700 m^3 of water. This leak triggered a response only in well MW-6, where the water table rose about 1 m to a steady position of 1,463 m. The second leak began January 5, 2012 and was stopped on May 15, 2012 after releasing 7,400 m^3 of water. The perched water table near MW-6 rose 4 to 1,465 m above sea level, and near well 33-3 rose 2 to 1,464 m. The third leak began March 2, 2013 and was stopped on May 20, 2013 after releasing 12,900 m^3 of water. The perched water table near MW-6 rose 4.5 to 1,464 m above sea level, and near well 33-3 rose 1.5 to 1,464.5 m.

References

Anderson SR (1991) Stratigraphy of the unsaturated zone and uppermost part of the Snake River Plain aquifer at the Idaho Chemical Processing Plant and Test Reactors Area, Idaho National Engineering Laboratory, Idaho. US Geol Surv Water Resour Invest Rep 91-4010

Anderson SR, Lewis BD (1989) Stratigraphy of the unsaturated zone at the radioactive waste management complex, Idaho National Engineering Laboratory, Idaho. US Geol Surv Water Resour Invest Rep 89-4065

Anderson SR, Liszewski MJ (1997) Stratigraphy of the unsaturated zone and the Snake River Plain aquifer at and near the Idaho National Engineering Laboratory, Idaho. US Geol Surv Water Resour Invest Rep 97-4183

Anderson SR, Ackerman DJ, Liszewski MJ, Freiburger RM (1996a) Stratigraphic data for wells at and near the Idaho National Engineering Laboratory, Idaho. US Geol Surv Open-File Rep 96-248

Anderson SR, Liszewski MJ, Ackerman DJ (1996b) Thickness of surficial sediment at and near the Idaho National Engineering Laboratory, Idaho. US Geol Surv Open-File Rep 96-330

Barraclough JT, Teasdale WE, Robertson JB, Jensen RG (1967) Hydrology of the National Reactor Testing Station, Idaho, 1966. US Geol Surv Open-File Rep 67-12

Bear J (1972) Dynamics of fluids in porous media. Dover, New York

Beven K, Germann P (2013) Macropores and water flow in soils revisited. Water Resour Res 49(6):3071–3092. doi: 10.1002/wrcr.20156

Burgess D (1995) Results of the neutron and natural gamma logging, stratigraphy, and perched water data collected during a large-scale infiltration test. EG&G ER, WAG7-60, EG&G Idaho, Las Vegas, NV

Cecil LD, Orr BR, Norton T, Anderson SR (1991) Formation of perched ground-water zones and concentrations of selected chemical constituents in water, Idaho National Engineering Laboratory, Idaho, 1986–88. US Geol Surv Water Resour Invest Rep 91-4166. http://pubs.er.usgs.gov/publication/wri914166. Accessed November 2016

Cuthbert MO, Mackay R, Nimmo JR (2013) Linking soil moisture balance and source-responsive models to estimate diffuse and preferential components of groundwater recharge. Hydrol Earth Syst Sci 17(3):1003–1019. http://www.hydrol-earth-syst-sci.net/17/1003/2013/hess-17-1003-2013.html. Accessed November 2016

Davis SN (1994) Vadose zone hydrogeology in the United States. In: Wilson LG, et al. (eds) Handbook of vadose zone characterization and monitoring. Lewis Publishers, London, pp 23–39

Duke CL, Roback RC, Reimus PW, Bowman RS, McLing TL, Baker KE, Hull LC (2007) Elucidation of flow and transport processes in a variably saturated system of interlayered sediment and fractured rock using tracer tests. Vadose Zone J 6(4): 855–867. doi:10.2136/vzj2006.0102

Dunnivant FM, Newman ME, Bishop CW, Burgess D, Giles JR, Higgs BD, Hubbell JM, Neher E, Norrell GT, Pfiefer MC, Porro I, Starr RC, Wyllie AH (1998) Water and radioactive tracer flow in a heterogeneous field-scale system. Ground Water 36(6):949–958

Ebel BA, Nimmo JR (2013) An alternative process model of preferential contaminant travel times in the unsaturated zone: application to Rainier Mesa and Shoshone Mountain, Nevada. Environ Model Assess 18(3):345–363. doi:10.1007/s10666-012-9349-8

Faybishenko B, Doughty C, Steiger M, Long J, Wood TR, Jacobsen JS, Lore J, Zawislanski PT (2000) Conceptual model of the geometry and physics of water flow in a fractured basalt vadose zone. Water Resour Res 36(12):3499–3520

Fayer MJ, Hillel D (1986) Air encapsulation: II. profile water storage and shallow water table fluctuations. Soil Sci Soc Am J 50:572–577

Forbes JR, Ansley SL (2008) INTEC groundwater monitoring report. DOE/ID-11356, DOE Idaho, Idaho Falls, ID. https://ar.icp.doe.gov/owa/getimage_2?F_PAGE=1&F_DOC=DOE/ID-11356&F_REV=1

Gerke HH, van Genuchten MT (1993) A dual-porosity model for simulating the preferential movement of water and solutes in structured porous media. Water Resour Res 29(2):305–319. doi:10.1029/92WR02339.

Hammermeister DP, Kling GF, Vomocil JA (1982) Perched water tables on hillsides in western Oregon: I. some factors affecting their development and longevity. Soil Sci Soc Am J 46(4):811–818

Healy R (2015) Simulating diffusive and preferential water flow in soils with a coupled source-Responsive/Richards-Equation Model. American Geophysical Union Fall Meeting, San Francisco, December 2015, AGU, Washington, DC

Hendrickx JMH, Flury M (2001) Uniform and preferential flow mechanisms in the vadose zone. In: National Research Council (ed) Conceptual models of flow and transport in the fractured vadose zone. National Academy Press, Washington, DC, pp 149–187

Heppner CS, Nimmo JR (2005) A computer program for predicting recharge with a master recession curve. US Geol Surv Water Resour Invest Rep 2005-5172

Hill DE, Parlange J-Y (1972) Wetting front instability in layered soils. Soil Sci Soc Am Proc 36(5):697–702

Hinds JJ, Ge S, Fridrich CJ (1999) Numerical modeling of perched water under Yucca Mountain, Nevada. Ground Water 37(4):498–504. doi:10.1111/j.1745-6584.1999.tb01135.x

Jarvis NJ (2007) A review of non-equilibrium water flow and solute transport in soil macropores: principles, controlling factors and consequences for water quality. Eur J Soil Sci 58(3):523–546. doi:10.1111/j.1365-2389.2007.00915.x

Knutson CF, McCormick KA, Smith RP, Hackett WR, O'Brien JP, Crocker JC (1990) FY 89 report: RWMC vadose zone basalt characterization. DOE-ID/EGG-WM-8949, DOE Idaho, Idaho Falls, ID

Kung KJS (1990) Preferential flow in a sandy vadose zone: 2. Mechanism and implications. Geoderma 46:59–71

Larsbo M, Jarvis N (2003) MACRO 5.0: a model of water flow and solute transport in macroporous soil—technical description. Studies in the Biogeophysical Environment, Emergo 2003:6, Swedish Univ. of Agricultural Sciences, Uppsala, Sweden

Lindholm GF (1996) Summary of the Snake River Plain regional aquifer-system analysis in Idaho and eastern Oregon. US Geol Surv Prof Pap 1408-A

Marinas M, Roy JW, Smith JE (2013) Changes in entrapped gas content and hydraulic conductivity with pressure. Groundwater 51(1):41–50

McElroy DL, Hubbell J (1990) Hydrologic and physical properties of sediments at the Radioactive Waste Management Complex. EGG-BG-9147, EG&G Idaho, Las Vegas, NV

Miller DE, Gardner WH (1962) Water infiltration into stratified soil. Soil Sci Soc Am Proc 26:115–119

Mirus BB, Nimmo JR (2013) Balancing practicality and hydrologic realism: a parsimonious approach for simulating rapid groundwater recharge via unsaturated-zone preferential flow. Water Resour Res 49(3):1458–1465. doi:10.1002/wrcr.20141

Mirus BB, Perkins KP, Nimmo JR (2011) Assessing controls on perched saturated zones beneath the Idaho Nuclear Technology and Engineering Center, Idaho. US Geol Surv Sci Invest Rep 2011-5222

Mualem Y (1976) A new model for predicting the hydraulic conductivity of unsaturated porous media. Water Resour Res 12(3):513–522

Nimmo JR (2007) Simple predictions of maximum transport rate in unsaturated soil and rock. Water Resour Res 43(5). doi:10.1029/2006WR005372

Nimmo JR (2010) Theory for source-responsive and free-surface film modeling of unsaturated flow. Vadose Zone J 9(2):295–306. doi:10.2136/vzj2009.0085

Nimmo JR, Malek-Mohammadi S (2015) Quantifying water flow and retention in an unsaturated fracture-facial domain. In: Faybishenko B et al (eds) Dynamics of fluids and transport in fractured porous systems. Geophysical Monograph 210, AGU, Washington, DC, pp 169–179

Nimmo JR, Mitchell L (2013) Predicting vertically nonsequential wetting patterns with a source-responsive model. Vadose Zone J 12(4)

Nimmo JR, Perkins KS (2008) Effect of soil disturbance on recharging fluxes: case study on the Snake River Plain, Idaho National Laboratory, USA. Hydrogeol J 16(5):829–844. doi:10.1007/s10040-007-0261-2

Nimmo JR, Perkins KS, Rose PA, Rousseau JP, Orr BR, Twining BV, Anderson SR (2002) Kilometer-scale rapid transport of naphthalene sulfonate tracer in the unsaturated zone at the Idaho National Engineering and Environmental Laboratory. Vadose Zone J 1:89–101

Nimmo JR, Rousseau JP, Perkins KS, Stollenwerk KG, Glynn PD, Bartholomay RC, Knobel LL (2004) Hydraulic and geochemical framework of the Idaho National Engineering and Environmental Laboratory vadose zone. Vadose Zone J 3(1):6–34, http://wwwrcamnl.wr.usgs.gov/uzf/abs_pubs/papers/vzj.3.6.pdf. Accessed November 2016

Oostrom M, Truex MJ, Carroll KC, Chronister GB (2013) Perched-water analysis related to deep vadose zone contaminant transport and impact to groundwater. J Hydrol 505:228–239

Orr BR (1999) A transient numerical simulation of perched ground-water flow at the test reactor area, Idaho National Engineering and Environmental Laboratory, Idaho, 1952-94. U.S. Geological

Survey Water-Resources Investigations Report 99-4277 (DOE/ID-22162), p 54

Perkins KS (2003) Measurement of sedimentary interbed hydraulic properties and their hydrologic influence near the Idaho Nuclear Technology and Engineering Center at the Idaho National Engineering and Environmental Laboratory. US Geol Surv Water Resour Invest Rep 03-4048. http://wwwrcamnl.wr.usgs.gov/uzf/abs_pubs/papers/WRI034048.pdf. Accessed November 2016

Perkins KS, Nimmo JR (2000) Measurement of hydraulic properties of the B-C interbed and their influence on contaminant transport in the unsaturated zone at the Idaho Engineering and Environmental Laboratory, Idaho. US Geol Surv Water Resour Invest Rep 00-4073

Perkins KP, Nimmo JR (2009) High-quality unsaturated zone hydraulic property data for hydrologic applications. Water Resour Res 45: W07417. doi:10.1029/2008WR007497

Perkins KS, Mirus BB, Johnson BD (2014) Measurement of Unsaturated Hydraulic Properties and Evaluation of Property-Transfer Models for Deep Sedimentary Interbeds, Idaho National Laboratory. US Geol Surv Sci Invest 2014-5026. http://pubs.usgs.gov/sir/2007/5093/. Accessed November 2016

Porro I, Bishop CW (1995) Large-scale infiltration test CPN data analysis, engineering design file, WAG7-58, INEL-95/040, DOE-ID, Idaho Falls, ID

Pruess K (1998) On water seepage and fast preferential flow in heterogeneous, unsaturated rock fractures. J Contam Hydrol 30:333–362

Rightmire CT, Lewis BD (1987) Hydrogeology and geochemistry of the unsaturated zone, Radioactive Waste Management Complex, Idaho National Engineering Laboratory, Idaho. US Geol Surv, Water Resour Invest 87-4198

Robinson BA, Broxton DE, Vaniman DT (2005) Observations and modeling of deep perched water beneath the Pajarito Plateau. Vadose Zone J 4(3):637–652. doi:10.2136/vzj2004.0168

Salve R, Rempe DM, Dietrich WE (2012) Rain, rock moisture dynamics, and the rapid response of perched groundwater in weathered, fractured argillite underlying a steep hillslope. Water Resour Res 48(11): W11528. doi:10.1029/2012WR012583

Smith RP (2004) Geologic setting of the Snake River Plain aquifer and vadose zone. Vadose Zone J 3(1):47–58, https://www.soils.org/publications/vzj/abstracts/3/1/47

Sorenson KS, Wylie AH, Wood TR (1996) Test area north hydrogeologic studies test plan: operable Unit 1-07B, I NEL-96/0105, DOE-ID, Idaho Falls, ID

Twining BV, Bartholomay RC, Hodges MKV (2014) Completion summary for boreholes USGS 140 and USGS 141 near the Advanced Test Reactor Complex, Idaho National Laboratory, Idaho. US Geol Surv Sci Invest 2014-5098

US Department of Energy (1989) Climatography of the Idaho National Engineering Laboratory. DOE/ID-12118, US Department of Energy Idaho Operations Office, Idaho Falls, ID

Winfield KA (2003) Spatial variability of sedimentary interbed properties near the Idaho Nuclear Technology and Engineering Center at the Idaho National Engineering and Environmental Laboratory. US Geol Surv Water Resour Invest Rep 03-4142. http://wwwrcamnl.wr.usgs.gov/uzf/abs_pubs/papers/WRI034048.pdf. Accessed November 2016

Wood T, Huang H (2015) Experimental and modeling studies of episodic air-water two-phase flow in fractures and fracture networks. In: Faybishenko B et al (eds) Fluid dynamics in complex fractured-porous systems. Wiley, Chichester, UK, pp 209–228

Wood TR, Norrell GT (1996) Integrated large-scale aquifer pumping and infiltration tests, groundwater pathways. Summary report, OU 7-06 INEL-96/0256, Lockheed Martin, Idaho Falls, ID